

## The Atmospheric Oxidizing Capacity in China: Part 2. Sensitivity to emissions of primary pollutants

5

Jianing Dai<sup>a</sup>, Guy P. Brasseur<sup>a,e,f</sup>, Mihalis Vrekoussis<sup>b,g,h</sup>, Maria Kanakidou<sup>b,d</sup>, Kun Qu<sup>b</sup>,  
Yijuan Zhang<sup>b</sup>, Hongliang Zhang<sup>c</sup>, Tao Wang<sup>f</sup>

10 <sup>a</sup> Environmental Modelling Group, Max Planck Institute for Meteorology, Hamburg, 20146,  
Germany

<sup>b</sup> Institute of Environmental Physics (IUP), University of Bremen, Bremen, 28359, Germany

<sup>c</sup> Department of Environmental Science and Engineering, Fudan University, Shanghai, 200433,  
China

15 <sup>d</sup> Environmental Chemical Processes Laboratory, Department of Chemistry, University of  
Crete, Heraklion, 70013, Greece

<sup>e</sup> National Center for Atmospheric Research, Boulder, Colorado, 80307, USA

<sup>f</sup> Department of Civil and Environmental Engineering, The Hong Kong Polytechnic University,  
Hong Kong, China

20 <sup>g</sup> Center of Marine Environmental Sciences (MARUM), University of Bremen, Bremen,  
28359, Germany

<sup>h</sup> Climate and Atmosphere Research Center (CARE-C), The Cyprus Institute, Nicosia, Cyprus

*Correspondence to:* Guy P. Brasseur (guy.brasseur@mpimet.mpg.de)

25

30

35

40

## Abstract

45 Despite substantial reductions in anthropogenic emissions, ozone ( $O_3$ ) pollution remains a  
severe environmental problem in urban areas of China. The reduction in the emission of  
pollutants affects formation of ozone through the changes in concentrations of  $O_3$  precursors  
and intermediates species as well as in the oxidation capacity of the atmosphere. However, the  
underlying mechanisms driving  $O_3$  changes are still not fully understood. Here, we employ a  
50 regional chemical transport model to quantify the changes in the formation of ozone as well as  
other secondary pollutants to a specified emission reduction (50%) for winter and summer  
conditions (January and July 2018). Our results indicate that, in winter, a 50% decrease in  
nitrogen oxide ( $NO_x$ ) emissions leads to an increase in surface  $O_3$  concentrations of 15%–33%  
on average across China. In summer, the concentration of  $O_3$  increases by up to 17% in the  
55 areas limited by the level of volatile organic compounds (VOCs), while it decreases by  
3%–12% in  $NO_x$ -limited areas. The increase in the ozone concentration is associated with a  
reduced  $NO_x$ -titration effect and higher levels of hydroxyl (OH) due to a reduced loss from  
reactions with nitrogen dioxide ( $NO_2$ ). With a 50% reduction in anthropogenic VOCs  
(AVOCs) emissions, the  $O_3$  concentration decreases across the entire geographic area, with  
60 reductions of 4%–10% in South China during winter and 8%–20% in urban areas during  
summer. When combining the reductions in  $NO_x$  and AVOCs emissions, the ozone response  
in urban areas (VOC-limited) is determined by the positive effect of  $NO_x$  emission reduction  
in winter and the negative effect of AVOCs emission reduction in summer. An exception is  
found in the response during summertime in South China, where the role of biogenic VOCs in  
65 ozone formation is crucial due to relatively high temperatures and the existence of vegetation  
surroundings.

Summertime increases in the concentration of oxidized VOCs (OVOCs), particularly  
aldehydes and alcohols, are attributable to the reduction in  $NO_x$  emissions. This enhancement  
70 subsequently enhances the atmospheric oxidative capacity through the photolysis of OVOCs  
and the oxidation of alkenes by OH radicals; it favors the formation of ozone. A significant  
decrease in particulate nitrate and in secondary organic aerosols is derived following the  
reduction in  $NO_x$  and AVOCs emissions, respectively. These reductions in the aerosol  
concentration contribute to  $O_3$  formation, through enhanced levels of hydroperoxyl ( $HO_2$ )  
75 radicals associated with a reduced loss via aerosol uptake, and a diminished aerosol extinction.

To effectively mitigate ozone pollution in urban areas, simultaneous reductions in the emission of NO<sub>x</sub> and specific VOCs species should be applied, especially regarding alkenes, aromatics, and unsaturated OVOCs, including methanol and ethanol.

80 Keywords: ozone pollution, emission reduction, WRF-Chem, AOC

## 1. Introduction

85

To effectively reduce air pollution in China, the government of the country has implemented stringent actions between 2013 and 2020 (Liu et al., 2020; Liu et al., 2023). In the initial phase, from 2013 to 2017, the control of primary pollutants was particularly effective, with a dramatic decrease in the anthropogenic emissions of fine particles (PM<sub>2.5</sub>), sulfur dioxide (SO<sub>2</sub>), and nitrogen oxides (NO<sub>x</sub>) (Zheng et al., 2018; Liu et al., 2020). In subsequent years, a sustained reduction in the emission of SO<sub>2</sub>, NO<sub>x</sub>, and PM<sub>2.5</sub> was achieved, particularly between 2018 and 2020 (Liu et al., 2023). The implementation of the emission control policies has greatly improved China's air quality. However, a significant increase in the surface ozone (O<sub>3</sub>) concentration was observed from 2013 to 2019, with the positive trend slowing down in 2020 and 2021, but rebounding in 2022 (Liu et al., 2023; China Air 2023). Several studies provide explanations for the positive trend observed in the surface O<sub>3</sub> concentration, including a reduction in the NO<sub>x</sub> emissions and in the atmospheric aerosol load (Li et al., 2019; Liu et al., 2020). During and after the recent COVID-19 lockdown period, ozone pollution has been reported to happen, which is believed to be favored by a sharp reduction of NO<sub>x</sub> and high emissions of volatile organic compounds (VOCs) (Li et al., 2021). Looking through these changes over the past decade, we learn that rapid reductions of emissions disturb substantially ozone chemistry and, thereby, produce changes in the ozone concentrations.

95

The response of ozone to reduced NO<sub>x</sub> emissions varies with the local photochemical environment and specifically with the encountered chemical regimes (i.e., VOC-limited, NO<sub>x</sub>-limited, or transition conditions) (Jacob., et al., 1995; Ou et al., 2016; Dai et al., 2023). In NO<sub>x</sub>-sensitive regimes, the reduction in NO<sub>x</sub> emissions decreases the number of NO<sub>2</sub> molecules photolyzed, leading to fewer ozone molecules being produced. While, in VOC-sensitive regimes, the reduction in the NO<sub>x</sub> abundance tends to enhance the ozone formation due to the weakening of NO titration and to the reduced loss of OH radical by the reaction with NO<sub>2</sub>. Several studies based on satellite observations (Wang et al., 2021) and regional models (Zhu et al., 2023) have shown that the reduction in anthropogenic emissions has generated a change in the geographical distribution of the ozone formation regimes in China. These studies have reported a shift of ozone sensitivity regimes from VOC-sensitive to transition and/or even to NO<sub>x</sub>-sensitive regimes in many metropolitan and suburban regions of East China. The shift towards NO<sub>x</sub>-limited conditions facilitates the implementation of an efficient ozone control

105

110

through the reduction in  $\text{NO}_x$  emissions only. In the remaining VOC-sensitive and transition areas,  $\text{NO}_x$  emission reduction fails to effectively mitigate ozone pollution. In this situation, a coordinated reduction in anthropogenic VOCs (AVOCs) emissions should be implemented to effectively limit the ozone formation (Liu et al., 2023; Zhu et al., 2023). The source of  $\text{NO}_x$  in VOC-sensitive areas is mainly from fossil fuel combustion, while the emissions of AVOCs emissions result from a broad range of industrial, transportation and residential sources (B. Li et al., 2021; C. Li et al., 2022). To establish a cost-effective control over AVOCs emissions, the contribution of different VOCs categories to ozone formation should be accurately quantified for different areas of China.

The effect of aerosols on the  $\text{O}_3$  formation has been considered in several modeling studies (Li et al., 2019; Liu et al., 2020). However, the influences of aerosol on the ozone production are complex due to the different effects that must be taken into consideration. (Tan et al., 2022; Dai et al., 2023). Understanding the changes in aerosol effects on the  $\text{O}_3$  formation, when the primary emissions are further reduced, remains a necessity for implementing successful air quality control policies.

Recent observational studies combined with a source apportionment approach using observation-based models have highlighted the role of anthropogenic VOCs species, including the alkenes, aromatics, and oxidized volatile organic compounds (OVOCs), for mitigating summertime ozone formation in the urban areas in China (C. Li et al., 2022; W. Wang et al., 2023). The notable contributions of OVOCs to the oxidizing capacity of the atmosphere (AOC) as well as the formation of secondary organic aerosols (SOA) have been a concern in the regions of Yangzi River Delta (YRD) (J. Li et al., 2022) and Pearl River Delta (PRD) (W. Wang et al., 2022). The important role of biogenic VOCs (BVOCs) has also been highlighted in vegetated rural and urban regions in China where the oxidation of BVOCs can significantly contribute to the formation of ozone and aerosols, specifically in the PRD region (J. Wang et al., 2023; Zhang et al., 2023). However, a comprehensive evaluation of the changes in the contribution of different VOCs categories to AOC and in ozone chemistry in response to emission changes in different regions of China is still needed. Considering the necessity of implementing coordinated actions in several large geographical areas to further alleviate air pollution in China, regional chemical transport models are appropriate tools to assess the quantitative response of secondary pollutants and of the oxidizing capacity of the atmosphere to emission changes.

In the companion paper (Part 1; Dai et al., 2023), we use a regional chemical-meteorological model to quantify the relative contribution of different photochemical processes to the formation and destruction of near-surface photochemical radicals and ozone in different chemical environments in China. In Part 2 of the study, with the evaluated model, we assess the response of the photo-oxidative species and related parameters to an imposed reduction of primary emissions. This paper is structured as follows. Section 2 introduces the setup of the model system and describes the simulations performed for specified reduction scenarios in the emissions of primary pollutants. In Section 3, we analyze the response of near-surface concentration of ozone to the specified emission reductions. Further, we determine the drivers responsible for the resulting ozone changes; these include changes in the concentrations of ozone precursors, of the intermediates including the oxidized VOCs (OVOCs) and in the level of secondary aerosols. We also discuss the changes to be expected in the ozone formation regimes. Finally, we describe the sensitivity of the atmospheric oxidative capacity (*AOC*) to the reduction in the emissions. A summary and implication for policy making of our study is provided in Sec. 4.

## 2. Method

### 2.1. Model setting

We use the WRF-Chem model version 4.1.2 (Skamarock et al., 2019), coupled with the gas-phase chemistry mechanism MOZART (Emmons et al., 2010) and the aerosol module MOSAIC (Zaveri et al., 2008), to simulate the meteorological fields as well as the transport, the chemical and physical transformations of trace gases and aerosols. The months of January and July of 2018 are selected as representative months to conduct the simulations and to investigate the changes in secondary pollution and in the *AOC* in response to emission reductions during winter and summer, respectively. Compared to the standard version of the chemical mechanism, several updates of heterogeneous uptake on the surface of the ambient aerosol were implemented (Dai et al., 2023). As for the SOA formation, the main pathways result from the gas-phase oxidation of VOCs by atmospheric oxidants (OH, O<sub>3</sub>, and NO<sub>3</sub>) and from the heterogeneous formation of glyoxal SOA over the ambient aerosol (Knote et al., 2014). The model domain covers the whole geographical area of China. Analyses of modeling results at four urban sites (Beijing, Shanghai, Guangzhou, and Chengdu) are also performed.

185 More detailed information on the model configuration, the model validation, and the sites selected for our analysis can be found in Part 1 of our paper Dai et al., (2023).

We adopt the Multi-resolution Emission Inventory (MEIC v1.3; <http://www.meicmodel.org/>) to represent anthropogenic emissions in China and the CAMS-GLOB-ANT v4.2 inventory (190 <https://eccad.aeris-data.fr/>) provided by the Copernicus Atmosphere Monitoring Service (CAMS) to account for the anthropogenic emissions in the Asian areas outside China. To explore the sensitivity of secondary pollution and of AOC to emission reduction, several sensitivity experiments are designed based on our emissions inputs of NO<sub>x</sub>, anthropogenic VOCs (AVOCs). As shown in Table S1 of the Supplementary Information, NO<sub>x</sub> emissions (195 include the emissions of NO<sub>2</sub> and NO, AVOCs emissions include those of alkanes [ethane (C<sub>2</sub>H<sub>6</sub>), propane (C<sub>3</sub>H<sub>8</sub>), and BIGALK (alkanes with carbon number ≥ 4)], alkenes [ethene (C<sub>2</sub>H<sub>4</sub>), propene (C<sub>3</sub>H<sub>6</sub>), and BIGENE (alkenes with carbon number ≥ 4)], aromatics [benzene (C<sub>6</sub>H<sub>6</sub>), toluene (C<sub>6</sub>H<sub>5</sub>CH<sub>3</sub>), and xylene (C<sub>6</sub>H<sub>4</sub>(CH<sub>3</sub>)<sub>2</sub>)], alkyne (C<sub>2</sub>H<sub>2</sub>), isoprene (C<sub>5</sub>H<sub>8</sub>), terpenes (C<sub>10</sub>H<sub>16</sub>), and OVOCs [methanol (CH<sub>3</sub>OH), ethanol (C<sub>2</sub>H<sub>5</sub>OH), acetaldehyde (200 (CH<sub>3</sub>CHO), acetone (CH<sub>3</sub>COCH<sub>3</sub>), methacrolein (CH<sub>2</sub>CCH<sub>3</sub>CHO; MACR), and methyl vinyl ketone (CH<sub>2</sub>CHCOCH<sub>3</sub>; MVK)]. The emissions of ammonia (NH<sub>3</sub>), sulfur dioxide (SO<sub>2</sub>), and carbon monoxide (CO) are also considered.

## 2.2. Design of numerical experiment

205 To explore the sensitivity of secondary pollutants to emissions changes, five numerical experiments are conducted for January and July of 2018, respectively (Table 1). In the baseline case, denoted as “BASE”, we adopt the emissions described in Sect. 2.1. The concentrations of the key species calculated in this specific case have been validated in our companion study (210 Dai et al., 2023). To quantify the sensitivity of pollutants to potential mitigation policies, we apply uniform reductions in the surface emissions of primary pollutants over the entire geographical area of China; In the first two cases, arbitrary 50% reductions are applied separately to the NO<sub>x</sub> and AVOCs emissions relative to the baseline case. These two cases are labeled “NO<sub>x</sub>” and “AVOCs”, respectively. A third case in which the 50% reduction is applied (215 to both NO<sub>x</sub> and AVOCs emissions is referred to as “N+A”. The difference between the “perturbed” concentrations of pollutants and chemical parameters relative to the baseline case provides an estimate of the response in secondary pollution and chemistry to emission reduction.

220 Additionally, a simulation labeled “*TOTAL*” assumes that all anthropogenic emissions under  
consideration ( $\text{NO}_x$ , AVOCs, CO,  $\text{SO}_2$ , and  $\text{NH}_3$ ) are simultaneously reduced by 50%. This  
particular case is used to explore the impact on the ozone formation of a reduction in the  
emission of CO (an ozone precursor) and of  $\text{SO}_2$  and  $\text{NH}_3$  (as aerosol precursors). The spatial  
distribution of the changes in the emission fluxes for the different cases is shown in Fig. S1.

225

### 3. Model results

#### 3.1 Response of ozone concentrations to emission reduction

230 First, we describe the changes in the surface concentration of ozone in response to the reduction  
applied to the surface emissions. To support the discussion, we adopt an indicator to distinguish  
different ozone sensitivity regimes. This indicator is defined as the calculated ratio between the  
production rate of hydrogen peroxide ( $\text{H}_2\text{O}_2$ ) and of nitric acid ( $\text{HNO}_3$ ) [ $P(\text{H}_2\text{O}_2)/P(\text{HNO}_3)$ ].  
An area is assumed to be VOC-limited or  $\text{NO}_x$ -limited if the adopted indicator  
235  $P(\text{H}_2\text{O}_2)/P(\text{HNO}_3)$  is smaller than 0.06 or if it is larger than 0.2, respectively (Tonnesen and  
Dennis, 2000; Yang et al., 2020; Zhao et al., 2019; Dai et al., 2023). The regions with ratios  
between these two limits represent transition situations.

Figure 1 displays the spatial distribution of the changes in the surface concentration of ozone  
240 during daytime (06:00 to 19:00 Local Standard Time) resulting from a 50% reduction in the  
emissions of  $\text{NO}_x$ , AVOCs, combined  $\text{NO}_x$  and AVOCs, and the additional reduction in other  
anthropogenic species ( $\text{NH}_3$ ,  $\text{SO}_2$ , and CO) for January and July 2018.

*Winter conditions.* In January, the 50% reduction in the  $\text{NO}_x$  emissions (*NO<sub>x</sub> case*) enhances  
245 the surface ozone concentrations, with the largest increase derived in the YRD and PRD  
regions by 15%–33% (6–12 ppbv; Fig. 1a). During wintertime, a large part of China is under  
a VOC-sensitive regime (Fig. S2a). The reduced ozone titration due to  $\text{NO}_x$  emission reduction  
leads to a decrease in ozone destruction (Fig. S3a) and hence favors an increase in the ozone  
concentration. If AVOCs emissions are reduced by 50% (*AVOCs case*), the surface ozone  
250 concentration is reduced by 4%–10% (2.0 to 8.0 ppbv; Fig. 1b) in South China. This ozone  
decrease is associated with reduced levels of radicals (see Sec. 3.2.1) and hence a reduction in  
the ozone production (Fig. S4a).



255 In the case with a combined emission reduction (*N+A* case), the ozone response in VOC-  
limited areas follows the positive changes found in the  $\text{NO}_x$ -reduction case, with an ozone  
increase of 4%–9% (3.0–7.5 ppbv; Fig. 1c) in North China and in some urban regions in South  
China. Simultaneously, a slight decrease in the ozone concentration is derived along the coast  
of South China (5%–8% or 2.0–4.5 ppbv). In these areas, the ozone sensitivity is under the  
control of the  $\text{NO}_x$ . The ozone decrease is dominated by the negative ozone response to the  
260 AVOCs emission reduction. With a further emission reduction for the other chemical species  
(*TOTAL* case), an ozone increase (4%–6% or 3–5 ppbv; Fig. 1d) relative to the combined case  
is calculated in South China.

*Summer conditions.* In July, under the reduction in the  $\text{NO}_x$  emissions, an increase in the  
265 surface ozone concentration of up to 17% (10 ppbv; Fig. 1e) is calculated in the urbanized  
regions of North China Plain (NCP), YRD, and PRD. These areas are typically located in VOC-  
limited areas (Fig. S2b); thus, the ozone increase is explained by the reduced ozone titration  
due to  $\text{NO}_x$  emission reduction. At the same time, in  $\text{NO}_x$ -limited areas, the calculated surface  
ozone concentration is reduced by 3%–10% (2 to 8 ppbv), in response to the reduced  
270 photochemical formation under lower  $\text{NO}_x$  concentrations. With the reduction of AVOCs  
emissions, the surface concentration of ozone decreases by 8%–20% (8.0–12.0 ppbv; Fig. 1f)  
in all areas of China.

In the combined emission reduction case, the surface concentration of ozone decreases by up  
275 to 15% (12 ppbv; Fig. 1g) in the  $\text{NO}_x$ -sensitive areas. In the VOC-sensitive areas, the surface  
ozone concentration also decreases, which differs from the ozone changes derived for winter  
conditions. This is explained by the fact that the loss of ozone due to  $\text{NO}_x$  titration is rapidly  
compensated by the photochemical formation of ozone, as the ozone production rate is  
enhanced by high temperatures and by large photolysis rates during summertime (T. Wang et  
280 al., 2022). When the emission reduction is applied to all species under consideration, the ozone  
changes (Fig. 1h) relative to the combined case are smaller than the changes derived in winter,  
due to a consistently smaller reduction in aerosol concentrations (see Sec. 3.2.3).

Table 2 and Figure S5 provide quantitative information on the response of ozone to emission  
285 reduction at four urban locations (Beijing, Shanghai, Chengdu, and Guangzhou) for January  
and July of 2018. In winter (in January), the reduction in the emission of  $\text{NO}_x$  results in ozone

increases of 21.3%–33.2% in all cities, while the reduction applied to AVOCs emission results in a decrease of urban ozone levels by 2.5%–18.2%. Ozone changes in the *N+A* and *TOTAL* cases follow the ozone response found in the *NO<sub>x</sub>* case, with concentration increases of 7.1%–22.0% and of 10.0%–22.7%, respectively. In summer (in July), the urban ozone responses to the *NO<sub>x</sub>* and *AVOCs* cases are similar to those derived for winter conditions. The calculated ozone concentrations increase by 5.5%–17.1% in response to the reduced *NO<sub>x</sub>* emissions and decrease by 14.5%–22.9% in response to the reduced *AVOCs* emissions. In the *N+A* and *TOTAL* cases, the changes in the ozone concentration follow the response to *AVOCs* reductions: the ozone concentration decreases at the sites of Beijing (by 5.5% and by 7.3%), Shanghai (by 2.9% and 2.6%), and Chengdu (by 3% and 2.5%). An exception is found at the Guangzhou site, where the ozone concentration increases by 1.3% in both cases; this calls for a different role of the anthropogenic emissions regarding the ozone formation at this location.

## 3.2. Changes in precursors and intermediates in ozone formation

In this section, we describe the changes in the surface concentration of ozone precursors and intermediates in response to the reduction in surface emissions. We focus in particular on the hydroxyl radical (OH), the hydroperoxyl radical (HO<sub>2</sub>), specific oxidized volatile organic compounds (OVOCs) species, as well as secondary aerosols

### 3.2.1. Changes in radicals

To support the discussion on the radical changes induced by the emission reduction, we examine the changes in the values of two specific parameters: the production rate of peroxy radicals ( $RO_x = OH + HO_2 + RO_2$ ;  $P(RO_x)$ ) and the destruction rate of these radicals ( $D(RO_x)$ ) (Tan et al., 2019). The production rate of  $RO_x$  radicals ( $P(RO_x)$ ) includes the photolysis of O<sub>3</sub>, of nitrous acid (HONO), and of different OVOCs species, as well as the ozonolysis of alkenes. The destruction rate of  $RO_x$  radicals ( $D(RO_x)$ ) results from the termination reactions between different  $RO_x$  radicals, and between  $RO_x$  radicals and nitric oxide. Another loss process for hydroperoxy radicals is provided by the heterogeneous uptake of HO<sub>2</sub> on aerosol surfaces. Detailed model estimates of  $P(RO_x)$  and  $D(RO_x)$  can be found in Part 1 of the present study (Dai et al., 2023).

320 *Winter conditions.* Figure 2 displays the spatial distribution of the changes in the surface  
daytime (06:00 to 19:00 LST) mixing ratios of OH and HO<sub>2</sub> radicals resulting from a 50%  
reduction in the emissions of NO<sub>x</sub>, AVOCs, combined NO<sub>x</sub> and AVOCs, and additional species  
(NH<sub>3</sub>, SO<sub>2</sub>, and CO) for January 2018. With the reduction in NO<sub>x</sub> emissions (*NO<sub>x</sub> case*), the  
325 calculated mixing ratio of the surface OH radical is reduced in South China by up to 40% (0.05  
pptv; Fig. 2a), with a lower decrease in the central and western parts of the country. The  
reduction in the levels of the OH radical are due to the reduced oxidative capacity of the  
atmosphere associated with the NO<sub>x</sub> emission reduction. The reduction in the atmospheric  
oxidative capacity is attributable to the decreases in the concentration of NO<sub>2</sub> (Fig. S6a) and of  
ozone.

330  
At the same time, an increase in the mixing ratios of OH radicals is found in urban areas,  
including the NCP, YRD, PRD, and Si Chuan Basin (SCB) regions, with a maximum increase  
of 24% in the PRD region. Consistently, at the four city sites under consideration, the highest  
increase in the level of the OH radical is found at the Guangzhou site (Figure S7). This increase  
335 results from the reduced loss of the OH radical by the reaction with NO<sub>2</sub> (Fig. S6b).

A distinct increase in the surface mixing ratio of the HO<sub>2</sub> radical is derived in South China; it  
reaches 5 pptv or 60% (Fig. 2e). This increase contributes to a higher ozone level through the  
reaction between HO<sub>2</sub> and NO. The enhancement in the urban HO<sub>2</sub> concentration results from  
340 the increased levels of the OH radical via VOCs oxidation. The reduction in the aerosol load  
derived in South China as a result of the reduced NO<sub>x</sub> emission is responsible for the reduced  
loss of HO<sub>2</sub> by aerosol uptake (see Sect. 3.2.3).

For the 50% decrease in AVOCs emissions (*AVOCs case*), the mixing ratios of OH and HO<sub>2</sub>  
345 radicals are reduced in South China by 4%–12% (0.005–0.015 pptv; Fig. 2b) and by 20%–36%  
(1–3 pptv; Fig. 2f), respectively. The decrease in the levels of these radicals is related to the  
reduced oxidation rate of VOCs following the decrease in the emissions and hence in the  
concentrations of hydrocarbons (Fig. S8a). The production of RO<sub>x</sub> also decreases, especially  
from the reduced photolysis of formaldehyde (HCHO) and of other OVOCs (Fig. S8b, c), a  
350 consequence of the reduced AVOCs emissions. In the *AVOCs case*, the decreases in the radical  
levels and in the production rate of radicals explain the wintertime ozone decreases derived in  
South China. Simultaneously, a slight increase in the mixing ratio of the OH radical is derived.

This increase is related to the reduced extinction of solar radiation associated with the reduced aerosol load following the reduction in the AVOCs emissions.

355

When the 50% emission reduction in  $\text{NO}_x$  is combined with the 50% reduction in AVOCs emissions (*N+A* case), the distribution of changes in the OH radical is similar to the pattern induced by emission reduction in  $\text{NO}_x$  alone. However, a weakened increase is calculated, as the increase in the OH radical concentration with the reduced  $\text{NO}_x$  emissions is largely  
360 compensated by the decrease in the radical concentrations produced by the reduction in the AVOCs emissions. As shown in Fig. 2c, the maximum increase of the OH radical in urban China is reduced to 12% (from 40%). At the same time, the increases in the mixing ratio of the  $\text{HO}_2$  radicals is reduced to 20% (from 60%; Fig. 2g), with only a mild increase distributed along the coast of South China. This compensating effect of the combined emission reduction  
365 on the radical levels is also reflected in the changes of the ozone concentrations, highlighting a link between the variations in the concentration of photochemical radicals and in the formation rate of ozone.

When accounting for the additional reduction in the emissions of other anthropogenic species  
370 ( $\text{NH}_3$ ,  $\text{SO}_2$ , and CO) (*TOTAL* case), the mixing ratio of the OH radical is positively modified, relative to the results obtained in the combined case (*N+A* case). As shown in Fig. 2d, the mixing ratio of the OH radical is enhanced by up to 22% in the PRD and SCB regions. This increase is due to the reduced consumption of the OH radical by the reduced emissions and related concentrations of carbon monoxide (CO) (Fig. S9a and S1d). For the  $\text{HO}_2$  radicals, the  
375 additional reduction in the other emissions contributes to a larger mixing ratio, with a pronounced increase in South China (by up to 18%; Fig. 2h). This increase in the  $\text{HO}_2$  radical mixing ratio is due to the increased oxidation of the VOCs by the OH radical and the reduced aerosol uptake of  $\text{HO}_2$  associated with the decrease in the aerosol load. The consistent increase between the OH and  $\text{HO}_2$  radical levels and the ozone concentrations in South China reveals a  
380 positive relation between radical enhancement and ozone production.

*Summer conditions.* Figure 3 displays the spatial distribution of the changes in the daytime surface mixing ratio of the OH and  $\text{HO}_2$  radicals due to the applied reduction in the emissions of  $\text{NO}_x$ , AVOCs, combined  $\text{NO}_x$  and AVOCs, and additional species for July 2018. When  
385 applying a 50% reduction in the  $\text{NO}_x$  emissions, the mixing ratio of the OH radicals decrease in large parts of China, with the maximum decrease reaching 40% (0.15 pptv; Fig. 3a). The

decrease in the concentration of the OH radicals can also be explained by the reduced consumption of OH by the reaction with NO<sub>2</sub>, due to the reduced emissions of nitrogen oxides. The geographical area in which the concentration of OH radicals is reduced, covers a large  
390 fraction of China, including the northern provinces. This area is different from the wintertime situation, when the OH reduction was occurring only in South China. The concentration of the OH radical increases in the metropolitan areas, including in the YRD and PRD regions. A consistent increase in the concentrations of the OH radicals is also derived at the sites of Shanghai and Guangzhou (Fig. S7). Simultaneously, the surface mixing ratio of the HO<sub>2</sub> radical  
395 increases by 15%–20% (6–8 pptv; Fig. 3e) in the North China Plain, due to the reduced loss via aerosol uptake. The spatial shift in the distribution of radical changes from South China in winter to North China in summer is influenced by seasonal patterns of meteorological parameters, including temperature, water vapor abundance, and solar radiation intensity, which affect the atmospheric oxidative processes (Dai et al., 2023).

400  
When AVOCs emissions are reduced by 50%, the mixing ratio of the radicals in urban areas, including in the NCP, YRD, and PRD regions, decreases on average by 8–12% in the case of OH (0.03–0.05 pptv; Fig. 3b) and by 6%–10% in the case of HO<sub>2</sub> (3–5 pptv; Fig. 3f). When applying the combined 50% emission reduction in AVOCs and NO<sub>x</sub>, the changes in the patterns  
405 of the OH radical are similar to the distribution derived for the reduction in NO<sub>x</sub> emissions alone, but it is also partially offset by the counteracting effect of AVOCs emissions, as for winter conditions. As shown in Fig. 3c, the maximum increase in OH radical is reduced to 20% (from 40%) and the maximum decrease is reduced to 12% (from 30%). The counteracting effect of AVOCs emission reduction is also shown in the enhanced abundance of HO<sub>2</sub> radicals  
410 (Fig. 3g), with less than 6% (from 15%–20%) increases in the urban areas.

With an additional 50% reduction in other anthropogenic emissions, the changes in OH and HO<sub>2</sub> radicals relative to the results obtained in the combined case are smaller than the changes derived for winter conditions (Fig. 3d and h). This is due to the small decrease in aerosol load  
415 during summer (see Sec. 3.2.3).

### 3.2.2 Changes in OVOCs

Oxygenated hydrocarbons (OVOCs) originate from direct biogenic and anthropogenic surface  
420 emissions (primary source), and from the oxidation of primary hydrocarbons (secondary

source) in the atmosphere (W. Wang et al., 2022). The photolysis of OVOCs produces photochemical radicals, which enter into the formation of secondary pollutants and have a potential negative effect on ozone pollution mitigation.

425 *Winter conditions.* Figure 4 shows the spatial distribution of the calculated changes in total OVOCs due to a 50% reduction in the emission of NO<sub>x</sub>, AVOCs, combined NO<sub>x</sub> and AVOCs, and additional other species for January 2018. With the adopted reduction in NO<sub>x</sub> emission, the OVOCs concentration decreases in the non-urban areas of South China and increases in urbanized China (Fig. 4a), which is consistent with the changes derived for the mixing ratio of the OH radical. The highest increase in the OVOCs concentration is approximately 10% (2  
430 ppbv) in the urban areas of the YRD and PRD regions; it includes a significant increase in the concentration of formaldehyde (HCHO; Fig. S10a), followed by peroxyacetyl nitrate (PAN; Fig. S10b), and alcohols (CH<sub>3</sub>OH and C<sub>2</sub>H<sub>5</sub>OH; Fig. S10c), as the secondary formation of these OVOCs species is determined by the OH-related reactions (Emmons et al., 2010). At the four  
435 city sites under consideration, the highest increase in OVOCs is calculated at Shanghai and Guangzhou, with concentrations increasing by about 12% (1.8 ppbv; Fig. 4f) and 8% (1.2 ppbv; Fig. 4g), respectively. This increase in the concentration of OVOCs is consistent with the higher increase of OH radicals at these two sites (Fig. S7).

440 When the AVOCs emissions are reduced, the abundance of OVOCs is reduced in all regions of China (Fig. 4b), with the highest decrease found in the regions of PRD and SCB. At the four city sites under consideration (Fig. 4e-h), the decrease is most pronounced in the case of the concentration of ketones (see Table S2 for specific OVOCs speciation), including acetone (CH<sub>3</sub>COCH<sub>3</sub>), methyl vinyl ketone (CH<sub>3</sub>C(O)CHCH<sub>2</sub>), and methyl ethyl ketone  
445 (CH<sub>3</sub>CH<sub>2</sub>C(O)CH<sub>2</sub>CH<sub>3</sub>). The abundance of these species is reduced by nearly half, as the relevant ketones originate primarily from anthropogenic emissions. When combining the emission reduction of AVOCs and NO<sub>x</sub>, the decrease in OVOCs concentration resulting from the AVOCs emission reduction is further strengthened in large areas of China (Fig. 4c). With additional decreases in the other emissions, the OVOCs' concentration is enhanced by 2–4  
450 ppbv in whole China (Fig. 4d), which is consistent with the increased abundance of the OH radical resulting from a reduction in the NH<sub>3</sub>, SO<sub>2</sub>, and CO emissions.

*Summer conditions.* Figure 5 displays the spatial distribution of the changes in total OVOCs concentrations in response to a 50% reduction in the emission of NO<sub>x</sub>, AVOCs, combined NO<sub>x</sub>

455 and AVOCs, and additional species for July 2018. With a 50% reduction in  $\text{NO}_x$  emissions, a slight decrease in the OVOC's concentrations (0.5–1.5 ppbv or 3%–8%) is derived in South China (Fig. 5a), which is dominantly contributed by the decreases in the concentration of HCHO, glyoxal, and PAN (Fig. S11a-c). The decreases in these OVOCs species are due to a lower contribution from the secondary formation from OH-related reactions, as a consistent  
460 decrease is calculated for the changes in OH radical. However, in Central and North China, the calculated concentration of OVOCs generally increases (0.5–2.0 ppbv or 5%–8%). This increase is mainly contributed by the enhancement in the concentration of aldehydes (Fig. S12a) and alcohols (Fig. S12b). The increase of OVOCs species is possibly due to the enhanced contribution from the reactions between alkenes and isoprene, whose concentrations are increased (Fig. S12c, d), and enhanced oxidants. This result indicates that reducing  
465 anthropogenic emissions of aldehydes and alcohols may help offset the increase in OVOCs caused by the reduction in  $\text{NO}_x$  emissions.

With a 50% reduction in AVOCs emission, the OVOCs concentrations are significantly  
470 reduced in the NCP and SCB regions (by 20%–30% on average; Fig. 5b). Compared with the reduced OVOCs concentration (by 50%) in winter, the summertime response of OVOCs to the AVOCs emission reduction is smaller. Consistently, at the Beijing site (Fig. 5e), the decrease in OVOCs concentration is calculated by 30% (10 ppbv) on average, which is smaller than the decrease of 46% (5 ppbv) in winter. This seasonal difference is attributable to the higher  
475 photochemical formation of OVOCs during summertime, which is favored by the higher levels of temperature, solar radiation, as well as the temperature-dependent biogenic emissions. The smaller decrease in alcohols concentration (from 1.5 ppbv in winter to 0.5 ppbv in summer; Figure S13) is also supportive to our finding, as its summertime formation is highly dependent on the photochemically reactions with BVOCs (Zhang et al., 2023). Considering the  
480 increases in aldehydes and alcohols levels induced by reduced  $\text{NO}_x$  emission, this result also reveals a need to reduce the primary emissions of these two OVOCs to effectively control their negative impact on ozone pollution mitigation.

When the combined reduction in the emissions of AVOCs with  $\text{NO}_x$  is considered, a lower  
485 decrease (by 15%–26%; Fig. 5c) is found in the concentration of OVOCs in the geographical areas of China compared to the response derived for the individual reductions in the  $\text{NO}_x$  or AVOCs emissions. This response is consistent with the relevant changes in levels of OH radicals. When the emission reduction is applied to the other species under consideration, the

response of the OVOCs concentration to the reduced emissions is small (<2 ppbv or 5%; Fig. 490 5d).

### 3.2.3. Changes in aerosol

Figure 6 shows the changes in the average concentrations of secondary aerosol resulting from 495 a 50% reduction in the emission of NO<sub>x</sub>, AVOCs, combined NO<sub>x</sub> and AVOCs, and additional other species in January and July of 2018.

*Winter conditions.* In January, the 50% reduction applied to NO<sub>x</sub> leads to a large decrease in the aerosol load (10–18 μg m<sup>-3</sup> or 12%–20%; Fig. 6a) in Central and South China. The aerosol 500 decrease predominantly results from the decrease in the NO<sub>3</sub><sup>-</sup> abundance (Fig. S14a) linked to the reduced concentration of NO<sub>2</sub>, followed by the reduction in the concentration of NO<sub>4</sub><sup>+</sup> (Fig. S14b). A slight increase in the abundance of secondary organic aerosols (SOA) is derived in the urban areas of the NCP, YRD, and PRD regions (1–2 μg m<sup>-3</sup> or 3%–5%; Fig. S14c), which is consistent with the increase in the level of oxidants, including the ozone and OH radicals. 505 With a 50% reduction applied to AVOCs emissions, the changes in the aerosol concentration are smaller than with the 50% reduction applied to the NO<sub>x</sub> emissions. The corresponding aerosol decrease of less than 4% (5 μg m<sup>-3</sup>; Fig. 6b), predominantly results from the reduction in SOA concentrations (Fig. S15a). With a joint reduction in the emissions of NO<sub>x</sub> and AVOCs (Fig. 6c), the decrease in the aerosol burden is larger than from the separated decrease in the 510 individual emissions; this is explained by the fact that the increase in the concentration of SOA resulting from the reduced NO<sub>x</sub> emissions is compensated by the reduced AVOCs emissions.

With a further reduction applied to other emissions (*TOTAL* case), the decrease in the concentration of aerosol is deeply enhanced in South China (Fig. 6d). This results in large part 515 from the decrease in NO<sub>3</sub><sup>-</sup> particles (by 5 μg m<sup>-3</sup>; by Fig. S16c), followed by the decrease in the concentration of NH<sub>4</sub><sup>+</sup> (by 2 μg m<sup>-3</sup>; Fig. S16a), SO<sub>4</sub><sup>2-</sup> (by 1 μg m<sup>-3</sup>; Fig. S16b). The decreases in NH<sub>4</sub><sup>+</sup> and SO<sub>4</sub><sup>2-</sup> concentrations are due to the reduction in the concentration of their gas-phase precursors, NH<sub>3</sub> and SO<sub>2</sub>. The decrease in the abundance of NO<sub>3</sub><sup>-</sup> results from the formation of ammonium nitrate (NH<sub>4</sub>NO<sub>3</sub>) through the reaction of NH<sub>3</sub> with HNO<sub>3</sub> (Meng et al., 2022). This decrease in the aerosol burden explains the enhancement of HO<sub>2</sub> radicals since the aerosol uptake is reduced. This, in turn, promotes an increase in the ozone concentration in South China. At four city sites, the largest decrease in the aerosol 520



concentration is found at the Beijing site (Fig. S17), followed by the Chengdu site. This is attributed to the relatively high aerosol levels at these two locations. In our model, the concentrations of  $\text{NO}_2$  and  $\text{PM}_{2.5}$  are overestimated for the baseline conditions (Dai et al., 2023), which can possibly lead to an excessively high reduction in aerosol concentration, especially in the concentration of  $\text{NO}_3^-$ . This overestimation potentially affects the aerosol-related changes in the ozone formation.

*Summer conditions.* In July, the decrease in the aerosol load due to the emission reduction is much smaller than in winter. The reduction ranges from 1.5 to 5  $\mu\text{g m}^{-3}$  (Fig. 6e), from 2 to 6  $\mu\text{g m}^{-3}$  (Fig. 6f), from 4 to 7  $\mu\text{g m}^{-3}$  (Fig. 6g) and from 8 to 10  $\mu\text{g m}^{-3}$  (Fig. 6h), for the reduction in the  $\text{NO}_x$ , AVOCs,  $N+A$ , and *TOTAL* emissions conditions, respectively. As for ozone, the reduction in aerosols also undergoes a spatial shift, from South China in winter to North China in summer. This shift is consistent with the calculated changes in oxidants, hydrocarbons, and other gaseous aerosol precursors. The higher decrease in the aerosol load for the combined case also indicates that the reduction in AVOCs emission increases the efficiency of the aerosol decrease produced by the reduced  $\text{NO}_x$  emissions.

The aerosol effect on ozone formation has been discussed in several modeling studies (Li et al., 2019; Liu et al., 2020; Dai et al., 2023). Our results show that the reduction in primary emissions results in a large decrease in aerosol concentrations. The major contribution to the aerosol decreases results from the reduction in  $\text{NO}_x$  emissions, with a strengthened effect when combined with a reduction in the AVOCs emissions. This decrease in the aerosol burden weakens the aerosol extinction effect and therefore enhances the photochemical formation rate of radicals and ozone. As shown in Fig. S18a-d, the photolysis rate increases (by 5%-20%) in Central and South China during winter due to the aerosol decrease induced by the emission reductions. The highest increase in the photolysis rates results from the joint emission reduction in  $\text{NO}_x$  and AVOCs (Fig. S18c). The increase of the photolysis rates in summer is not as distinct as the increase during wintertime due to the limited reduction in the aerosol burden during summer (Fig. S18e-h).

Further, the reduction in the aerosol burden lowers the aerosol uptake of  $\text{NO}_2$  and  $\text{HO}_2$  radicals, which indirectly enhances the mixing ratio of OH and  $\text{HO}_2$  radicals (Dai et al., 2023). An increased level of  $\text{HO}_2$  radical following the emission reduction is caused by the reduced aerosol uptake. Large uncertainties still exist in the adopted value of the uptake coefficient of

HO<sub>2</sub> (considered as 0.1 in this study) (Yang et al., 2023). This affects the quantitative evaluation of the aerosol effects on the ozone levels and deserves further studies. Considering the impact of aerosol load on ozone formation, it is essential to account for the aerosol effect on ozone formation, even with stringent emission reductions in the future.

### 3.3. Response of ozone sensitivity regimes to emission reduction

Figure 7 displays the spatial distribution of ozone regimes in response to applied emission reductions for of NO<sub>x</sub>, AVOCs, for combined NO<sub>x</sub> and AVOCs (*N+A*), and for additional species (*TOTAL*) in January and July.

*Winter conditions.* In January, when a 50% reduction is applied to the NO<sub>x</sub> emissions, the regions characterizing the ozone production in the south and southwest of China (in *BASE* case; Fig. S2a) tend to be converted from transition or VOC-limited regimes to NO<sub>x</sub>-limited areas (from 68.8% in *BASE* case to 71.9% in *NOx* case; Table S3) (Fig. 7a). The change in the ozone sensitivity regimes is consistent with (1) the reduced HNO<sub>3</sub> concentration (Fig. S19a) due to less NO<sub>2</sub> reacting with OH, and (2) the enhanced H<sub>2</sub>O<sub>2</sub> concentration (Fig. S10e) due to the reduced aerosol HO<sub>2</sub> uptake by aerosol particles. With a 50% reduction applied to the AVOCs emissions, some transition areas of South China are converted to VOC-limited areas (Fig. 7b; from 20.1% in the *BASE* case to 21.3% in the *AVOCs* case). A relevant decrease in the H<sub>2</sub>O<sub>2</sub> concentration, derived in South China (Fig. S19f), is attributed to the decrease in the calculated HO<sub>2</sub> concentration. When considering the combined reduction in NO<sub>x</sub> and AVOCs emissions as well as the reduction in all anthropogenic emissions, the VOC-limited regions of South China evolve towards a transition region or even a NO<sub>x</sub>-limited region (Fig. 7c; Fig. 7d). In these two last cases, the changes in ozone sensitivity regimes are determined by the decrease in the calculated HNO<sub>3</sub> concentrations (Fig. S19c, d). At the urban sites, the emission reduction does not modify the wintertime ozone sensitivity regimes (Fig. S20), which remain VOC-limited.

*Summer conditions.* In July, the changes in ozone regimes related to emission reductions are found mainly in VOC-limited areas and their surroundings, due to consistent changes in H<sub>2</sub>O<sub>2</sub> and HNO<sub>3</sub> (Fig. S21). With the reduction of NO<sub>x</sub> emissions, the size of VOC-limited areas shrinks and becomes a smaller fraction of the urbanized areas (Fig. 7e; from 3.4% in the *BASE* case to 2.9% in the *NOx* case). The regimes at three urban sites, which are VOC-limited in the

*BASE* case, are modified: the ozone sensitivity at Beijing is converted to a  $\text{NO}_x$ -limited case (Fig. 7i), while the sites of Shanghai (Fig. 7j) and Chengdu (Fig. 7l) are shifted towards a Transition regime. The changes in ozone sensitivity at these three city sites result from the decreased production of  $\text{HNO}_3$  due to reduced  $\text{NO}_2$  as well as the increased production of  $\text{H}_2\text{O}_2$  due to reduced  $\text{HO}_2$  loss via aerosol uptake. The Guangzhou site remains in a VOC-limited region (Fig. 7k). Reasons for this exception can be the lower aerosol load (Fig. S17) and higher temperature-dependent biogenic VOCs emissions in the location (Dai et al., 2023), as its surroundings are covered by vegetations (Zhang et al., 2023).

With the reduction in AVOCs emissions, the VOC-limited areas expand to the surroundings of the metropolitan areas (Fig. 7g; 3.7% in *AVOCs* case). Finally, when applying a combined 50% reduction in the emissions of  $\text{NO}_x$  and AVOCs (*N+A* case; Fig. 7g) as well as the reduction of all other emitted species (*TOTAL* case; Fig. 7h), the patterns of the calculated change in the ozone sensitivity are similar to the pattern corresponding to the  $\text{NO}_x$  emissions; specifically, the VOC-limited area (3.0% in *N+A* and *TOTAL* case) becomes smaller relative to the *BASE* case. In these cases, the sites of Beijing and Chengdu shift to a transition condition, while the Guangzhou and Shanghai sites remain under VOC-limited conditions. This result is consistent with the ozone increase obtained for the *N+A* and *TOTAL* cases at the Guangzhou sites.

### 3.4. Changes in Atmospheric Oxidative Capacity

The atmospheric oxidizing capacity (*AOC*) characterizes the self-cleansing ability of the atmosphere (Dai et al., 2023). This parameter is expressed as:

$$AOC = \sum_i^j k_{i,j} [Y_i] [X_j].$$

Here the  $k_{i,j}$  represents the reaction rate between carbon monoxide (CO), methane ( $\text{CH}_4$ ), and non-methane hydrocarbons (NMHCs) (noted here as  $Y_i$ ) and the OH radical, the  $\text{NO}_3$  radical as well as  $\text{O}_3$  (noted as  $X_j$ ).

The changes in the spatial distribution of daytime (06:00 to 19:00 LST) *AOC* resulting from the adopted 50% reduction in the emissions of ozone precursors for January and July of 2018 are depicted in Fig. 8.

625 *Winter conditions.* In January, the 50% reduction in  $\text{NO}_x$  emission leads to a decrease in  
daytime *AOC* of 10%–20% in South China and an increase of 10%–18% in the urban areas,  
including the PRD, YRD and, SCB regions (Fig. 8a). At the four city sites (Fig. 9a-d), the  
increase in the daytime *AOC* is attributed to the enhanced contributions of the OH-related  
630 reactions, including the reactions of OH with alkenes, followed by the reaction of OH with  
OVOCs and with aromatics. This daytime increase in *AOC* is consistent with the enhanced  
level in the OH radical, alkenes, and OVOCs when the  $\text{NO}_x$  emissions are reduced. The change  
in *AOC* with  $\text{NO}_x$  emission reduction allows us to characterize the formation process of  $\text{O}_3$  and  
can be used as an indicator to design mitigation policies for reducing ozone pollution. During  
nighttime (20:00 to 05:00 LST), the reduction in  $\text{NO}_x$  emissions is responsible for an increase  
635 in *AOC* by up to 50% (Fig. S22a). A contribution to this increase is provided by the alkenes'  
ozonolysis, since the concentration of ozone (Fig. 6a) and of alkenes is enhanced (Fig. S12c).  
The largest increase in the alkene ozonolysis (from 31% to 40%, see Fig. S23b) is derived at  
the site of Shanghai. These results highlight the enhanced oxidative processes associated with  
the  $\text{NO}_x$  emission reduction.

640  
With the 50% reduction in AVOCs emissions, the daytime *AOC* is reduced in all the major  
regions of China (Fig. 8b), with the largest decreases occurring in the southern part of the  
country; specifically, the largest decrease occurs at the Guangzhou site (by 50%). This decrease  
in daytime *AOC* is mainly attributable to the reduced contribution from the reactions between  
645 OH and alkenes, followed by the reactions of OH with aromatics and with OVOCs. With a  
combined reduction in the emissions of  $\text{NO}_x$  and AVOCs (*N+A*; Fig. 8c), the distribution  
patterns of the changes in daytime *AOC* are similar to the patterns found in the AVOCs cases  
but are characterized by higher decreases in daytime *AOC*. With the additional reduction in the  
other emissions considered here (*TOTAL*; Fig. 8d), an increase (relative to the *BASE* case) of  
650 daytime *AOC* is derived in central and south China; this result is consistent with the increase  
of OH radical levels and of the ozone concentrations.

*Summer conditions.* During summertime, the decrease in daytime *AOC* is more pronounced  
than during wintertime. With the 50% reduction applied to  $\text{NO}_x$  emissions, the daytime *AOC*  
655 decreases in large areas of China (ranging from 10%–20%; Fig. 8e), while, in urban areas, an  
increase is predicted, including at the Guangzhou (8%; Fig. 9g), Shanghai (5%; Fig. 9f), and  
Chengdu (3%; Fig. 9h) sites. However, at the Beijing site, the daytime value of *AOC* decreases

(Fig. 9e), because of the shift in the ozone sensitivity regime (from VOC-limited to NO<sub>x</sub>-limited conditions). During nighttime, the NO<sub>x</sub> emission reduction also leads to an increase in AOC due to the alkene ozonolysis (Fig. S22b), with the largest increase derived at the Beijing site (from 10% to 14%; Fig. S23e).

With other emission reduction cases (AVOCs and N+A; Fig. 8f, g), the daytime AOC decreases in entire China, with more distinct decreases (relative to winter conditions) occurring in North China. With the reduction in the AVOCs emissions, the relative decrease of daytime AOC is smaller than in winter, especially at the Guangzhou site (to 30%), indicating a more important secondary formation of VOC-related AOC during summer. When the emissions of NO<sub>x</sub> and AVOCs are jointly reduced by 50%, the role of the reaction between OH and BVOCs in the determination of AOC is enhanced at the four city sites, with the largest increase (15%) found at the Guangzhou site. This increase results from the enhanced levels of OH radicals (Fig. 2c) and in the presence of biogenic VOCs species, such as isoprene (Fig. S24).

The distribution patterns of changes in daytime AOC due to emission reduction are largely consistent with the changes in the mixing ratio of the OH radicals and the changes in the concentration of OVOCs, ozone, and SOA in both winter and summer. These consistent patterns suggest that the AOC is an appropriate indicator to characterize the changes in secondary pollutants attributed to emission reduction. One exception is found when considering the changes in the ozone concentration resulting from the reduction in NO<sub>x</sub> emissions during winter. During this season, a comparison between the values of daytime AOC and the changes in the ozone concentration (Fig. 5a) suggests that the change in daytime AOC reflects primarily the changes in the net production rate of odd oxygen (Fig. S25); this can be explained by the important role played by NO<sub>2</sub> in the wintertime formation of ozone.

#### 4. Summary and Policy Implications

The model simulations performed in the present study explore the response of radicals, ozone, and the atmospheric oxidative processes to a 50% reduction applied to the primary emissions of key pollutants. Our analysis provides insight into the changes affecting ozone chemistry and the oxidizing processes to be expected in response to future emission reduction.

*In winter*, as most geographical areas are VOC-limited (saturated in NO<sub>x</sub>) a 50% reduction in NO<sub>x</sub> emissions leads to an ozone concentration increase of up to 8–10 ppbv (15%–25%) in all geographical regions of China; this increase results from the reduced titration of ozone by nitric oxide. When combining this NO<sub>x</sub> reduction with a 50% reduction applied to AVOCs emissions, the ozone enhancement found in the rural areas and resulting from the reduced NO<sub>x</sub> is considerably reduced. However, in urban areas (VOC-limited situation), the ozone increase, although weakened, still exists (by 3.0–7.5 ppbv).

*In summer*, as most rural areas of China become NO<sub>x</sub>-limited, the geographical regions covered by the ozone increase in response to the 50% reduction applied to the NO<sub>x</sub> emissions shrink almost to the VOC-limited metropolitan areas. In these urban environments, the ozone increase reaches a maximum of 10 ppbv or 17%. When the NO<sub>x</sub> emission reduction is combined with a 50% reduction in the VOC emissions, the increase in ozone almost disappears in all areas of China. This is explained by the significant decrease in the ozone production resulting from the reduced levels of hydrocarbons. However, in the areas where hydrocarbons are primarily of biological origin, the ozone concentration (i.e., linked to the photochemical degradation of isoprene) still slightly increases (i.e., by 0.5 ppbv or 1.3% at the Guangzhou sites).

*Paths to mitigation.* We conclude this paper by highlighting a few chemical paths that should be considered when designing mitigation policies for the reduction of ozone in the urban areas of China. Figure 10 presents a schematic description of the chemical mechanisms involved in the chemical production of atmospheric ozone, and highlights how different reaction paths tend to change the ozone abundance in response to a reduction in NO<sub>x</sub> and anthropogenic VOC (AVOCs) emissions. This graph shows that a reduction in NO<sub>x</sub> emissions tends to increase the ozone concentration by (1) reducing the rate of the NO + O<sub>3</sub> reaction (ozone titration); (2) by increasing the rate of the HO<sub>2</sub> + NO reaction due to an increase in the HO<sub>2</sub> level associated with the reduced uptake of this radical by a lowered aerosol load; (3) by increasing the atmospheric oxidizing capacity (AOC) through OH-related reactions. The graph also shows that a decrease in AVOCs emissions tends (1) to reduce the level of the HO<sub>x</sub> radical and hence the ozone production by the HO<sub>2</sub> + NO reaction; (2) to enhance the level of OH radical due to the reduced aerosol uptake and (3) to reduce the AOC with a negative change of the ozone concentration. The relative importance of these different chemical mechanisms varies with location and environmental conditions.

725 We conclude that in *winter*, when the background ozone concentration is low, the reduction of  
NO<sub>x</sub> emissions tends to increase the level of near-surface ozone, while the reduction in AVOCs  
emissions has the opposite effect. This conclusion applies both in rural and in urban areas. A  
combined reduction in the emissions of these two primary pollutants tends to decrease the level  
of ozone in rural areas but to increase ozone in urban areas. Thus, in urban areas during winter,  
730 an effective approach to reduce the surface ozone concentration is through a strong limitation  
in the emissions of volatile organic compounds.

In *summer* when the ozone level is generally high, the reduction of NO<sub>x</sub> emissions is an  
effective action to reduce the ozone concentration in rural areas. This measure, however, is  
735 counterproductive in the NO<sub>x</sub>-saturated urban areas where ozone is controlled by VOCs. In  
fact, in urban areas during this season, the mechanisms involved in ozone mitigation are  
complex. For example, when NO<sub>x</sub> emissions are reduced, the atmospheric OH concentration is  
enhanced because of its reduced destruction by NO<sub>2</sub>. Following this increase in the OH  
concentration, an increase in the level of OVOCs, whose photolysis is an important source of  
740 HO<sub>x</sub> radicals, also leads to accelerated ozone production and further amplifies the oxidation of  
VOCs. In addition, the increase in AOC, linked to the reactions of OH and ozone with alkenes  
and the reactions of OH with OVOCs also contribute to an increase in the ozone production.  
Further, the reduction in the aerosol load, resulting from a reduction in the emissions of aerosol  
precursors, promotes ozone formation by decreasing the aerosol extinction of light and by  
745 reducing the uptake of HO<sub>2</sub>. If combined with a 50% reduction in AVOCs, the increase in the  
OVOCs concentrations and AOC, resulting from reduced NO<sub>x</sub> emissions, can be offset.  
However, the aerosol-related promotion of the level of OH and HO<sub>2</sub> radicals can be enhanced,  
highlighting the complexity of summertime ozone mitigation in urban areas.

750 In urban areas, the reduction in the level of surface ozone requires a reduction in the emissions  
of anthropogenic VOCs. However, for practical reasons, a 50% reduction in AVOCs emissions,  
as assumed in our study, will be difficult to implement over a short period of time. With the  
known contribution of the VOCs-related reactions to the AOC, the reduction in the emissions  
of alkenes, aromatics, and unsaturated OVOCs, especially methanol and ethanol, should be a  
755 priority. The development of efficient mitigation strategies based on the reduction of AVOCs  
emissions requires, however, more detailed investigations on the reactivity of individual VOCs  
and on their potential impact on the ozone formation.

760 **Code and data availability.** The WRF-Chem model is publicly available at  
<https://www2.mmm.ucar.edu/wrf/users/>. The modified code in the WRF-Chem model is  
available upon request to the corresponding author. The air quality data at surface stations are  
publicly available at the website of the Ministry of Ecology and Environment of the People's  
Republic of China at <http://english.mee.gov.cn/>.

765 **Author contributions.** JD and GB designed the structure of the manuscript, performed the  
numerical experiments, analyzed the results, and wrote the manuscript. JD analyzed the data  
and established the figures. All co-authors provided comments and reviewed the manuscript.

770 **Competing interests.** The authors declare that they have no conflict of interest.

**Acknowledgments.** The present joint Sino-German study was supported by the German  
Research Foundation (Deutsche Forschungs Gemeinschaft DFG), the National Science  
Foundation of China (NSFC) under Air-Changes grant no. 4487-20203, the Research Grants  
Council– University Grants Committee (grant no. T24-504/17-N) and the NSFC (grant  
775 no.42293322). The National Center for Atmospheric Research (NCAR) is sponsored by the  
US National Science Foundation. We would like to acknowledge the high-performance  
computing support from NCAR Cheyenne.

## References

- 780 China Air 2023, Air Pollution Prevention and Control Progress in Chinese Cities.  
<http://www.allaboutair.cn/uploads/231027/ChinaAir2023EN.pdf>
- 785 Dai, J., Brasseur, G. P., Vrekoussis, M., Kanakidou, M., Qu, K., Zhang, Y., Zhang, H., and  
Wang, T.: The atmospheric oxidizing capacity in China – Part 1: Roles of different  
photochemical processes, *Atmos. Chem. Phys.*, 23, 14127–14158, <https://doi.org/10.5194/acp-23-14127-2023>, 2023.
- 790 Emmons, L. K., Walters, S., Hess, P. G., Lamarque, J.-F., Pfister, G. G., Fillmore, D., Granier,  
C., Guenther, A., Kinnison, D., Laepple, T., Orlando, J., Tie, X., Tyndall, G., Wiedinmyer, C.,  
Baughcum, S. L., and Kloster, S.: Description and evaluation of the Model for Ozone and  
Related chemical Tracers, version 4 (MOZART-4), *Geosci. Model Dev.*, 3, 43–67,  
<https://doi.org/10.5194/gmd-3-43-2010>, 2010.
- 795 Jacob, D. J., Horowitz, L. W., Munger, J. W., Heikes, B. G., Dickerson, R. R., Artz, R. S., and  
Keene, W. C.: Seasonal transition from NO<sub>x</sub> - to hydrocarbon-limited conditions for ozone  
production over the eastern United States in September, *J. Geophys. Res.-Atmo.*, 100, 9315–  
9324, <https://doi.org/10.1029/94JD03125>, 1995.
- 800 Knote, C., Hodzic, A., Jimenez, J. L., Volkamer, R., Orlando, J. J., Baidar, S., Brioude, J., Fast,  
J., Gentner, D. R., Goldstein, A. H., Hayes, P. L., Knighton, W. B., Oetjen, H., Setyan, A.,  
Stark, H., Thalman, R., Tyndall, G., Washenfelder, R., Waxman, E., and Zhang, Q.: Simulation



of semi-explicit mechanisms of SOA formation from glyoxal in aerosol in a 3-D model, *Atmos. Chem. Phys.*, 14, 6213–6239, <https://doi.org/10.5194/acp-14-6213-2014>, 2014.

805

Li, B., Ho, S.S.H., Li, X., Guo, L., Chen, A., Hu, L., Yang, Y., Chen, D., Lin, A., Fang, X., A comprehensive review on anthropogenic volatile organic compounds (VOCs) emission estimates in China: comparison and outlook. *Environ. Int.* 156, 106710, <https://doi.org/10.1016/j.envint.2021.106710>, 2021.

810

Li, C., Liu, Y., Cheng, B., Zhang, Y., Liu, X., Qu, Y., Feng, M.: A comprehensive investigation on volatile organic compounds (VOCs) in 2018 in Beijing, China: Characteristics, sources and behaviors in response to O<sub>3</sub> formation. *Sci. Total Environ.*, 806, 150247 <https://doi.org/10.1016/j.scitotenv.2021.150247>, 2022.

815

Li, J., Xie, X., Li, L., Wang, X., Wang, H., Jing, S. A., Hu, J.: Fate of Oxygenated Volatile Organic Compounds in the Yangtze River Delta Region: Source Contributions and Impacts on the Atmospheric Oxidation Capacity. *Environ. Sci., Technol.*, 56(16), 11212–11224. <https://doi.org/10.1021/acs.est.2c00038>, 2022.

820

Li, K., Jacob, D. J., Liao, H., Shen, L., Zhang, Q., Bates, K. H.: Anthropogenic drivers of 2013–2017 trends in summer surface ozone in China. *Proc. Natl. Acad. Sci.*, 116 (2), 422–427, <https://doi.org/10.1073/pnas.1812168116>, 2019.

825

Li, K., Jacob, D. J., Liao, H., Qiu, Y., Shen, L., Zhai, S., Kuk, S. K.: Ozone pollution in the North China Plain spreading into the late-winter haze season. *Proc. Natl. Acad. Sci.*, 118(10), e2015797118, <https://doi.org/10.1073/pnas.2015797118>, 2021.

830

Liu, T., Hong, Y., Li, M., Xu, L., Chen, J., Bian, Y., Yang, C., Dan, Y., Zhang, Y., Xue, L., Zhao, M., Huang, Z., and Wang, H.: Atmospheric oxidation capacity and ozone pollution mechanism in a coastal city of southeastern China: analysis of a typical photochemical episode by an observation-based model, *Atmos. Chem. Phys.*, 22, 2173–2190, <https://doi.org/10.5194/acp-22-2173-2022>, 2022.

835

Liu, Y., Geng, G., Cheng, J., Liu, Y., Xiao, Q., Liu, L., Zhang, Q.: Drivers of Increasing Ozone during the Two Phases of Clean Air Actions in China 2013–2020. *Environ. Sci., Technol.*, <https://doi.org/10.1021/acs.est.3c00054>, 2023

840

Liu, Y., and Wang Tao: Worsening urban ozone pollution in China from 2013 to 2017 – Part 2: The effects of emission changes and implications for multi-pollutant control, *Atmos. Chem. Phys.*, 20, 6323–6337, <https://doi.org/10.5194/acp-206323>, 2020.

845

Meng, F., Zhang, Y., Kang, J., Heal, M. R., Reis, S., Wang, M., Liu, L., Wang, K., Yu, S., Li, P., Wei, J., Hou, Y., Zhang, Y., Liu, X., Cui, Z., Xu, W., and Zhang, F.: Trends in secondary inorganic aerosol pollution in China and its responses to emission controls of precursors in

- wintertime, *Atmos. Chem. Phys.*, 22, 6291–6308, <https://doi.org/10.5194/acp-22-6291-2022>, 2022.
- 850 Ou, J., Yuan, Z., Zheng, J., Huang, Z., Shao, M., Li, Z., Louie, P. K.: Ambient ozone control in a photochemically active region: short-term despiking or long-term attainment? *Environ. Sci., Technol.*, 50 (11), 5720-5728, <https://doi.org/10.1021/acs.est.6b00345>, 2016.
- 855 Skamarock, W.C., Klemp, J.B., Dudhia, J., Gill, D.O., Liu, Z., Berner, J., Wang, W., Powers, J.G., Duda, M.G., Barker, D.M.: A Description of the Advanced Research WRF Model Version 4; Mesoscale and Microscale Meteorology Laboratory NCAR: Boulder, CO, USA, 2019.
- 860 Song, H., Lu, K., Dong, H., Tan, Z., Chen, S., Zeng, L., Zhang, Y.: Reduced aerosol uptake of hydroperoxyl radical may increase the sensitivity of ozone production to volatile organic compounds. *Environ. Sci., Technol. Lett.*, 9(1), 22-29. <https://doi.org/10.1021/acs.estlett.1c00893>, 2021.
- 865 Tan, Z., Lu, K., Hofzumahaus, A., Fuchs, H., Bohn, B., Holland, F., Liu, Y., Rohrer, F., Shao, M., Sun, K., Wu, Y., Zeng, L., Zhang, Y., Zou, Q., Kiendler-Scharr, A., Wahner, A., and Zhang, Y.: Experimental budgets of OH, HO<sub>2</sub>, and RO<sub>2</sub> radicals and implications for ozone formation in the Pearl River Delta in China 2014, *Atmos. Chem. Phys.*, 19, 7129–7150, <https://doi.org/10.5194/acp-19-7129-2019>, 2019.
- 870 Tan, Z., Lu, K., Ma, X., Chen, S., He, L., Huang, X., Zhang, Y.: Multiple Impacts of Aerosols on O<sub>3</sub> Production Are Largely Compensated: A Case Study Shenzhen, China. *Environ. Sci., Technol.*, 56(24), 17569-17580, <https://doi.org/10.1021/acs.est.2c06217>, 2022.
- 875 Tonnesen, G. S., and R. L. Dennis.: Analysis of radical propagation efficiency to assess ozone sensitivity to hydrocarbons and NO<sub>x</sub>: 2. Long-lived species as indicators of ozone concentration sensitivity, *J. Geophys. Res.*, 105(D7), 9227–9241, <https://doi.org/10.1029/1999JD900372>, 2000.
- 880 Wang, J, Zhang Y, Xiao S, Wu Z, Wang X.: Ozone Formation at a Suburban Site in the Pearl River Delta Region, China: Role of Biogenic Volatile Organic Compounds. *Atmosphere*, 14 (4):609. <https://doi.org/10.3390/atmos14040609>, 2023.
- 885 Wang, T., Xue, L., Feng, Z., Dai, J., Zhang, Y., Tan, Y.: Ground-level ozone pollution in China: a synthesis of recent findings on influencing factors and impacts. *Environ. Res. Letters*, 17(6), 063003. <https://doi.org/10.1088/1748-9326/ac69fe>, 2022.
- 885 Wang, W., van der A, R., Ding, J., van Weele, M., and Cheng, T.: Spatial and temporal changes of the ozone sensitivity in China based on satellite and ground-based observations, *Atmos. Chem. Phys.*, 21, 7253–7269, <https://doi.org/10.5194/acp-21-7253-2021>, 2021.

- 890 Wang, W., Yuan, B., Peng, Y., Su, H., Cheng, Y., Yang, S., Wu, C., Qi, J., Bao, F., Huangfu,  
Y., Wang, C., Ye, C., Wang, Z., Wang, B., Wang, X., Song, W., Hu, W., Cheng, P., Zhu, M.,  
Zheng, J., and Shao, M.: Direct observations indicate photodegradable oxygenated volatile  
organic compounds (OVOCs) as larger contributors to radicals and ozone production in the  
atmosphere, *Atmos. Chem. Phys.*, 22, 4117–4128, <https://doi.org/10.5194/acp-22-4117-2022>,  
2022.
- 895 Xue, L., Gu, R., Wang, T., Wang, X., Saunders, S., Blake, D., Louie, P. K. K., Luk, C. W. Y.,  
Simpson, I., Xu, Z., Wang, Z., Gao, Y., Lee, S., Mellouki, A., and Wang, W.: Oxidative  
capacity and radical chemistry in the polluted atmosphere of Hong Kong and Pearl River Delta  
region: analysis of a severe photochemical smog episode, *Atmos. Chem. Phys.*, 16, 9891–9903,  
900 <https://doi.org/10.5194/acp-16-9891-2016>, 2016.
- Yang, G., Liu, Y., Li, X. Spatiotemporal distribution of ground-level ozone in China at a city  
level. *Sci Rep* 10, 7229, <https://doi.org/10.1038/s41598-020-64111-3>, 2020.
- 905 Yang, L. H., Jacob, D. J., Colombi, N. K., Zhai, S., Bates, K. H., Shah, V., Beaudry, E.,  
Yantosca, R. M., Lin, H., Brewer, J. F., Chong, H., Travis, K. R., Crawford, J. H., Lamsal, L.  
N., Koo, J.-H., and Kim, J.: Tropospheric NO<sub>2</sub> vertical profiles over South Korea and their  
relation to oxidant chemistry: implications for geostationary satellite retrievals and the  
observation of NO<sub>2</sub> diurnal variation from space, *Atmos. Chem. Phys.*, 23, 2465–2481,  
910 <https://doi.org/10.5194/acp-23-2465-2023>, 2023.
- Zaveri, R. A., R. C. Easter, J. D. Fast, and L. K. Peters, Model for Simulating Aerosol  
Interactions and Chemistry (MOSAIC), *J. Geophys. Res.*, 113, D13204,  
doi:10.1029/2007JD008782, 2008
- 915 Zhang, Y., Dai, J., Li, Q., Chen, T., Mu, J., Brasseur, G., Wang, T., Xue, L.: Biogenic volatile  
organic compounds enhance ozone production and complicate control efforts: Insights from  
long-term observations in Hong Kong. *Atmos. Environ.*, 309, 119917,  
<https://doi.org/10.1016/j.atmosenv.2023.119917>, 2023.
- 920 Zhao, X., Zhou, W., and Han, L.: Human activities and urban air pollution in Chinese mega  
city: An insight of ozone weekend effect in Beijing, *Phys Chem Earth Pt. A/B/C*, 110, 109–  
116, <https://doi.org/10.1016/j.pce.2018.11.005>, 2019.
- 925 Zheng, B., Tong, D., Li, M., Liu, F., Hong, C., Geng, G., Li, H., Li, X., Peng, L., Qi, J., Yan,  
L., Zhang, Y., Zhao, H., Zheng, Y., He, K., and Zhang, Q.: Trends in China's anthropogenic  
emissions since 2010 as the consequence of clean air actions, *Atmos. Chem. Phys.*, 18, 14095–  
14111, <https://doi.org/10.5194/acp-18-14095-2018>, 2018
- 930 Zhu, S., Ma, J., Wang, S., Sun, S., Wang, P., Zhang, H.: Shifts of formation regimes and  
increases of atmospheric oxidation led to ozone increase in North China Plain and Yangtze  
River Delta from 2016 to 2019. *J. Geophys. Res.: Atmos.*, e2022JD038373,  
<https://doi.org/10.1029/2022JD038373>, 2023.

935

940

Table 1. Sensitivity experiments

Model Experiments	Description <sup>a</sup>
<i>BASE</i>	Without emission reduction
<i>NO<sub>x</sub></i>	With emission reduction in NO <sub>x</sub> by a factor of 2
<i>AVOCs</i>	With emission reduction in anthropogenic VOCs by a factor of 2
<i>N+A</i>	With emission reduction in NO <sub>x</sub> and anthropogenic VOCs by a factor of 2
<i>TOTAL</i>	With emission reduction in all considered species by a factor of 2

945 <sup>a</sup> Relevant species in emission inputs is shown in Sect. 2.1 and Table S1 in Supplementary  
Materials.

950

955

960

965

970

975

Table 2. Percentage changes of surface ozone due to emission reduction in urban location

980

Location	Sites	Ozone changes in winter condition (Mean $\pm$ SD)			
		$NO_x^a$	$AVOCs^b$	$N+A^c$	$TOTAL^d$
North	Beijing	25.0 $\pm$ 25.2 <sup>c</sup>	-2.5 $\pm$ 1.3	22.0 $\pm$ 32.8	20.0 $\pm$ 19.5
East	Shanghai	33.2 $\pm$ 35.3	-18.2 $\pm$ 13.5	21.8 $\pm$ 20.5	22.7 $\pm$ 18.8
South	Guangzhou	21.4 $\pm$ 22.6	-17.1 $\pm$ 11.2	7.1 $\pm$ 3.2	10.0 $\pm$ 3.5
West	Chengdu	21.3 $\pm$ 23.8	-9.4 $\pm$ 8.5	14.1 $\pm$ 8.3	20.3 $\pm$ 13.5
Location	Sites	Ozone changes in summer condition (Mean $\pm$ SD)			
		$NO_x$	$AVOCs$	$N+A$	$TOTAL$
North	Beijing	6.4 $\pm$ 3.8	-21.8 $\pm$ 19.2	-5.5 $\pm$ 4.2	-7.3 $\pm$ 5.0
East	Shanghai	17.1 $\pm$ 12.8	-22.9 $\pm$ 20.8	-2.9 $\pm$ 2.1	-2.6 $\pm$ 1.5
South	Guangzhou	15.0 $\pm$ 13.1	-14.5 $\pm$ 13.5	1.3 $\pm$ 1.0	1.3 $\pm$ 0.9
West	Chengdu	5.5 $\pm$ 4.5	-14.5 $\pm$ 10.2	-5.5 $\pm$ 2.0	-4.5 $\pm$ 1.9

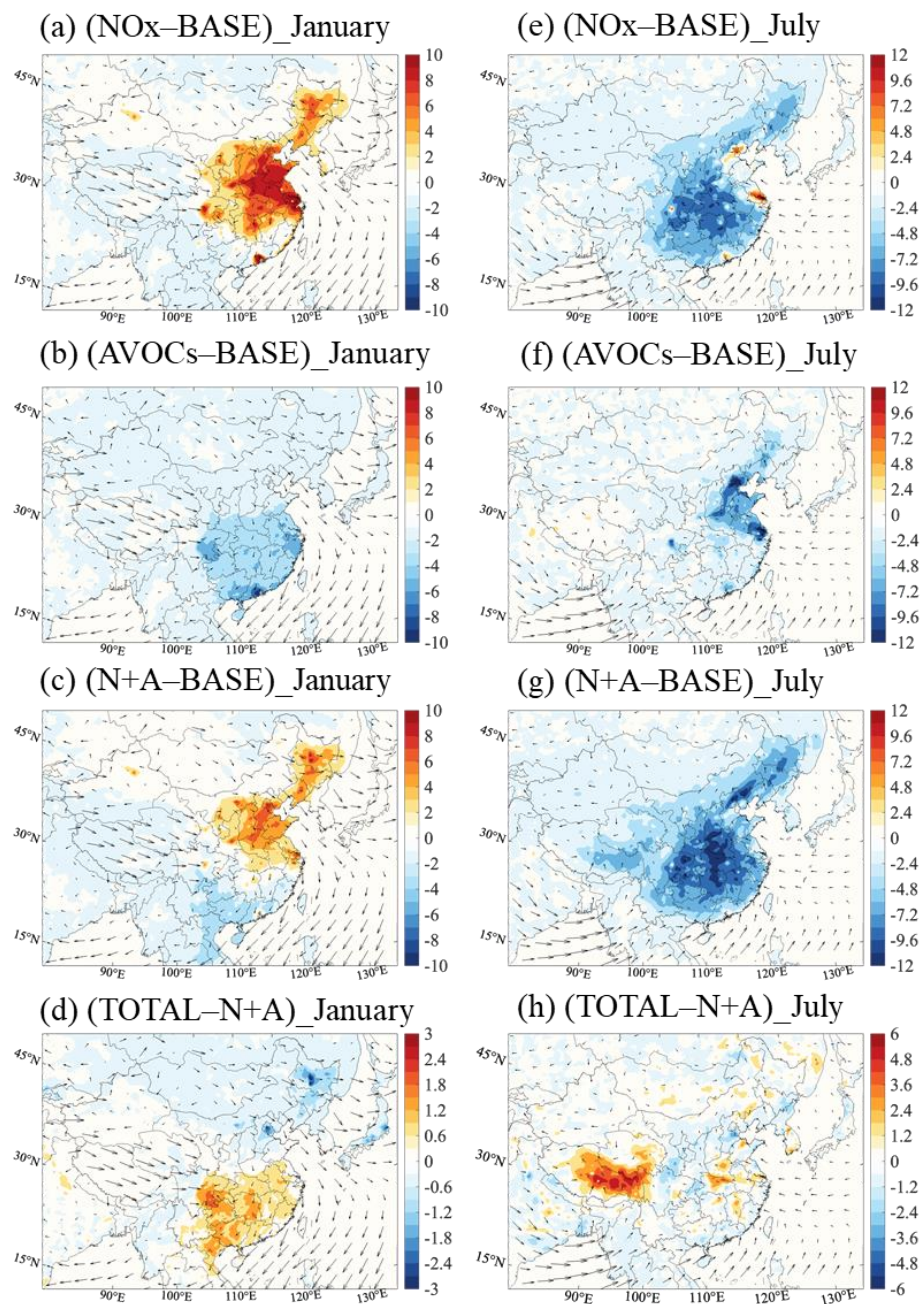
a-d. Sensitivity cases with a 50% reduction in the emissions of  $NO_x$  ( $NO_x$ ),  $AVOCs$  ( $AVOCs$ ),  $NO_x$  and  $AVOCs$  ( $N+A$ ), and other species ( $NO_x$ ,  $AVOCs$ ,  $CO$ ,  $NH_3$ ,  $SO_2$ ) under consideration ( $TOTAL$ ).

985

e. Values are displayed in the average ozone changes during daytime (06:00 to 19:00 LST) in percentage with the standard deviation as the error bar. (ozone changes= (case value – base value)/base value  $\times$ 100).

990

995

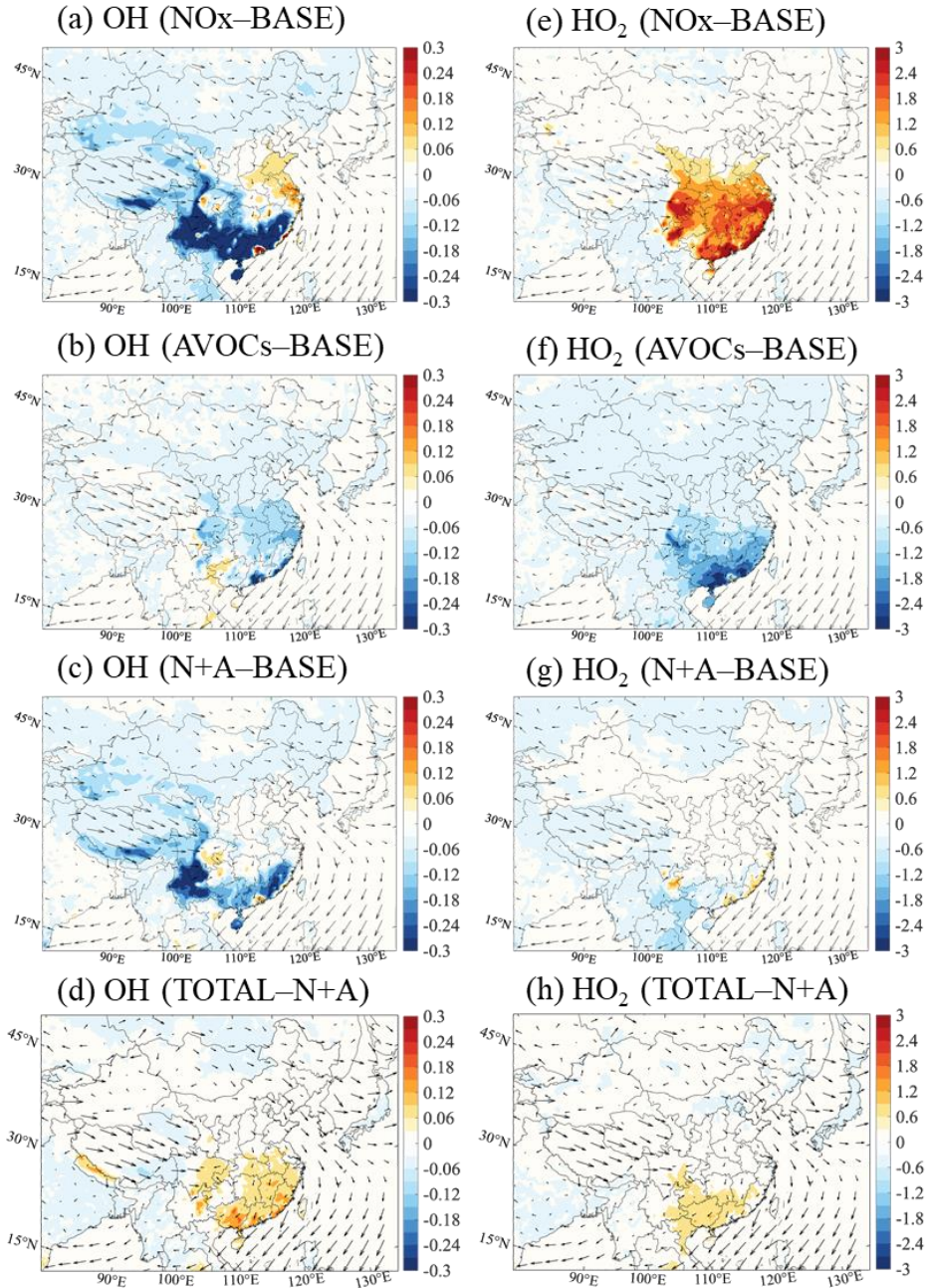


1000

1005

Figure 1. Changes in the monthly-averaged daytime (06:00 to 19:00 LST) surface ozone concentration (Unit: ppbv) response to a 50% reduction in  $\text{NO}_x$  emissions (a, e;  $\text{NO}_x$  case), in anthropogenic VOCs (AVOCs) emissions (b, f; AVOCs case) and in combined  $\text{NO}_x$  and AVOCs emissions (c, g;  $N+A$  case) relative to *BASE* case and to the additional reduction in the emission of  $\text{CO}$ ,  $\text{NH}_3$  and  $\text{SO}_2$  by 50% (d, h; *TOTAL* case) relative to  $N+A$  case for January (a-d) and July (e-h) 2018. Arrows represent the wind speed and wind direction. Notice the inconsistency in the scale of Figure 1d and 1h.





1010

Figure 2. Changes in the monthly-averaged daytime (06:00 to 19:00 LST) surface mixing ratio of OH radical (a-d, Unit: 0.1 pptv) and HO<sub>2</sub> radical (e-h, Unit: pptv) response to a 50% reduction in the emissions of NO<sub>x</sub> (a, e; *NO<sub>x</sub>* case), anthropogenic VOCs (b, f; *AVOCs* case) and in NO<sub>x</sub> and AVOCs (c, g; *N+A* case) relative to *BASE* case and in additional emission reduction of other species (d, h; *TOTAL* case) relative to *N+A* case for January of 2018. Arrows represent the wind speed and wind direction.

1020

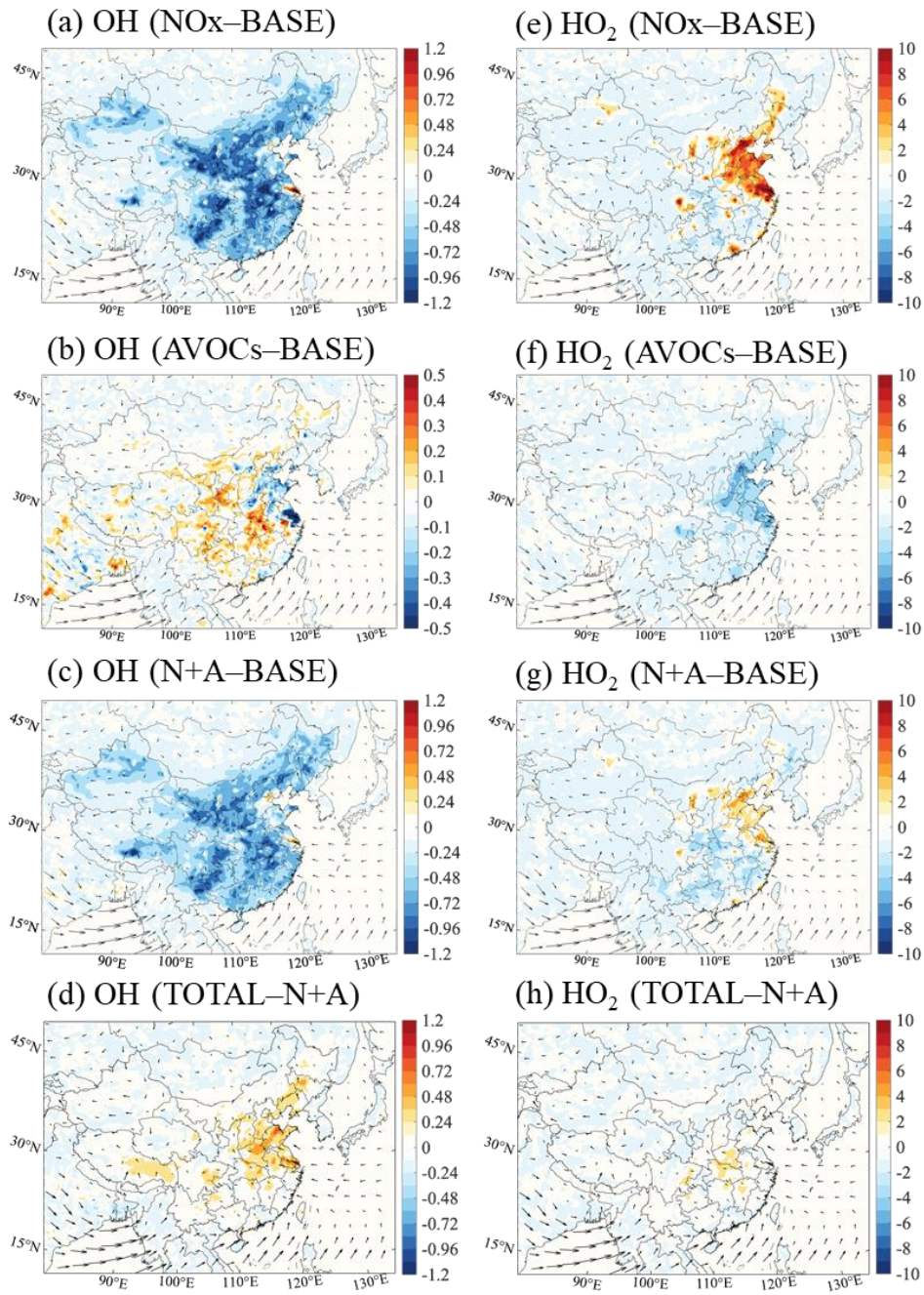
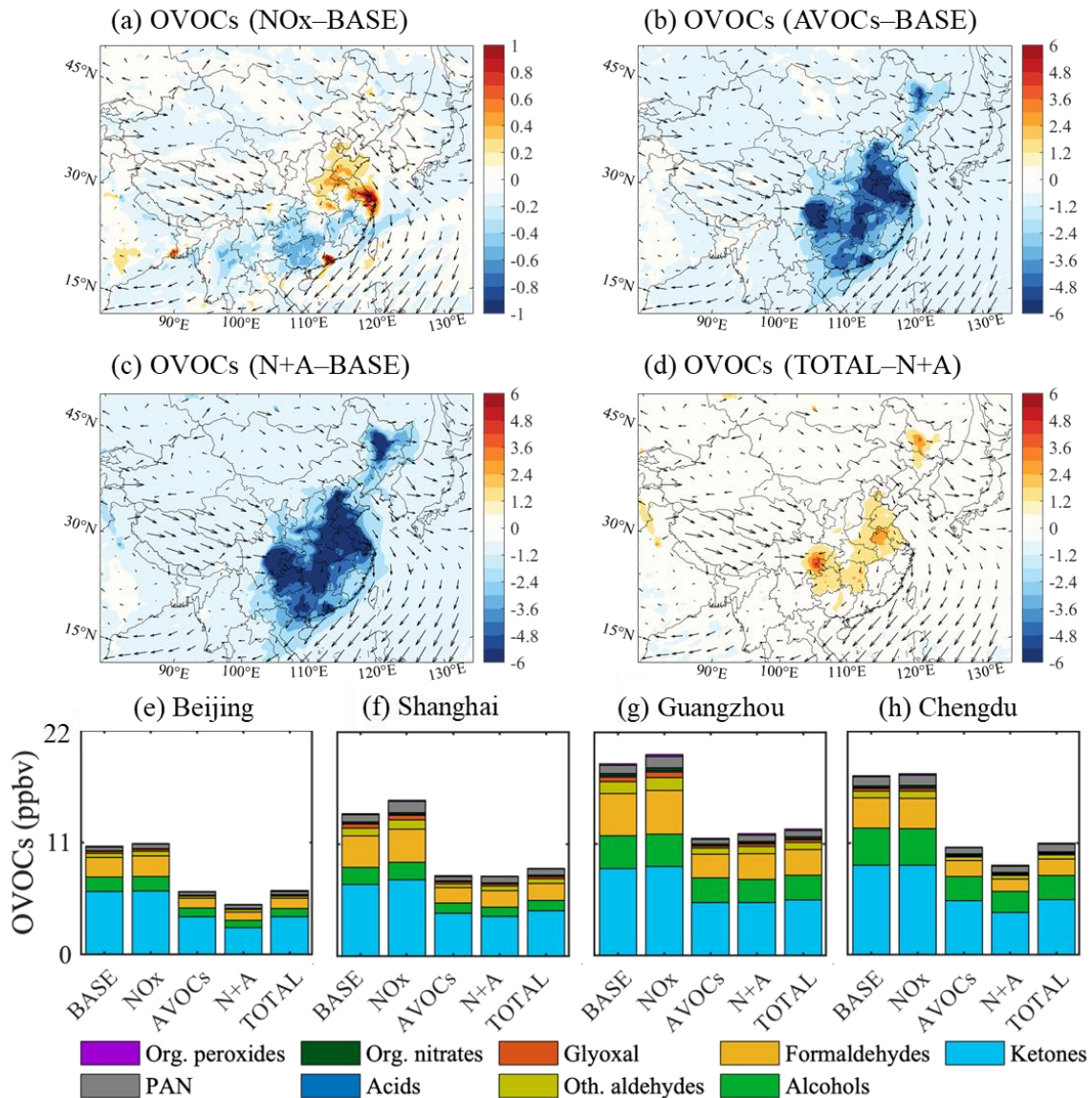


Figure 3. Same as Fig.2 but for July of 2018. Notice the inconsistency in the scale of Figure 2b.

1025

1030





1035 Figure 4. Changes in the monthly-averaged surface concentration of total oxidized VOCs (OVOCs) for January 2018. (a-d) Changes in the concentration of total OVOCs (Unit: ppbv) response to the reduction in the emission of  $\text{NO}_x$  (a,  $\text{NO}_x$  case), anthropogenic VOCs (b,  $\text{AVOCs}$  case) and combined  $\text{NO}_x$  and  $\text{AVOCs}$  (c,  $\text{N+A}$  case) relative to the  $\text{BASE}$  case and in an additional emission reduction of other species (d,  $\text{TOTAL}$  case) relative to  $\text{N+A}$  case. (e-h) Averaged concentration of OVOCs contributed by different species at four city sites (Beijing, Shanghai, Guangzhou, and Chengdu) in China in five simulated cases ( $\text{BASE}$ ,  $\text{NO}_x$ ,  $\text{AVOCs}$ ,  $\text{N+A}$ , and  $\text{TOTAL}$  cases). Arrows in panel (a-d) represent the wind speed and wind direction. Notice the inconsistency in the scale of Figure 3a.

1040

1045

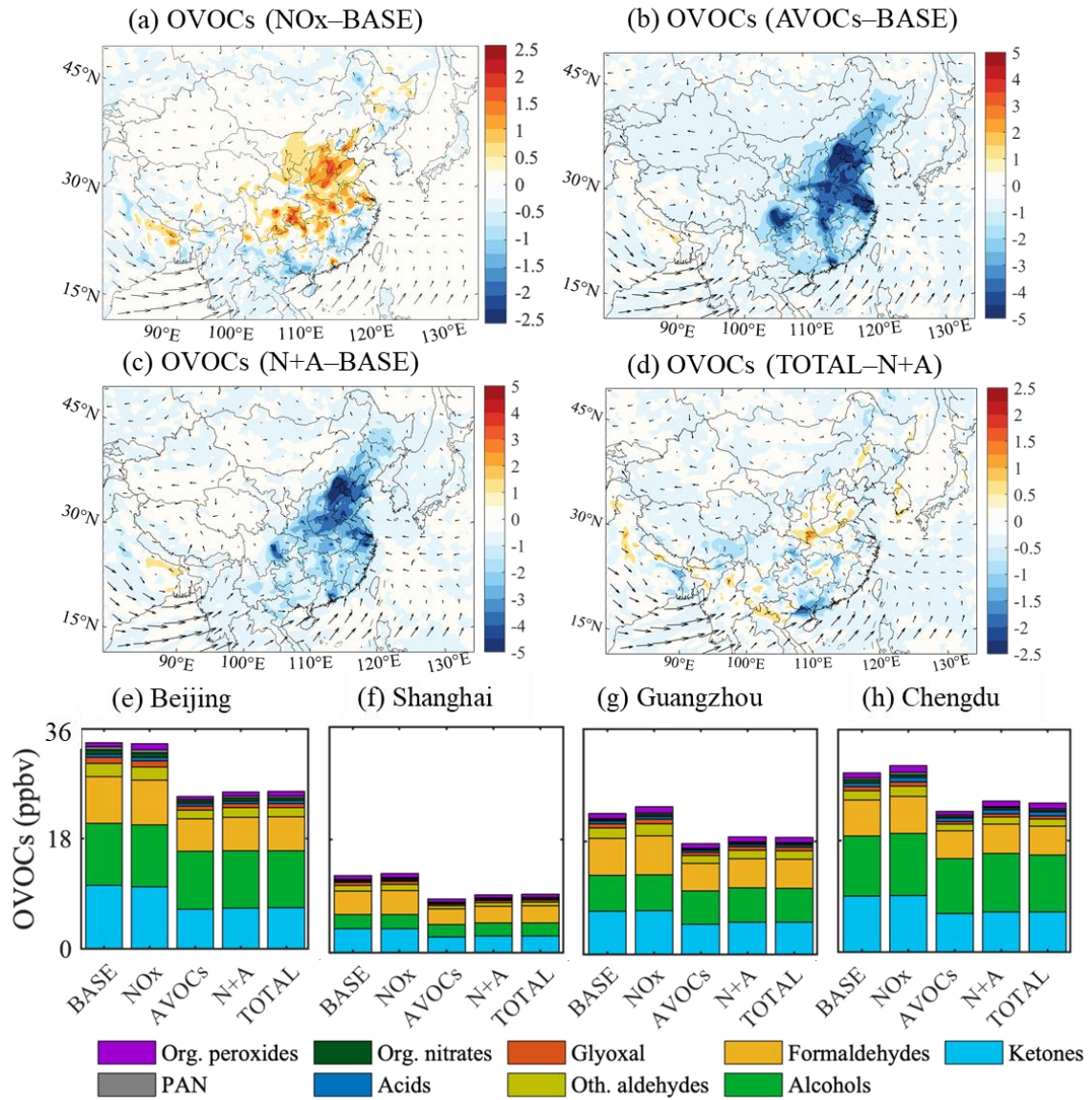


Figure 5. Same as Fig.4 but for July of 2018. Notice the inconsistency in the scale of Figure.

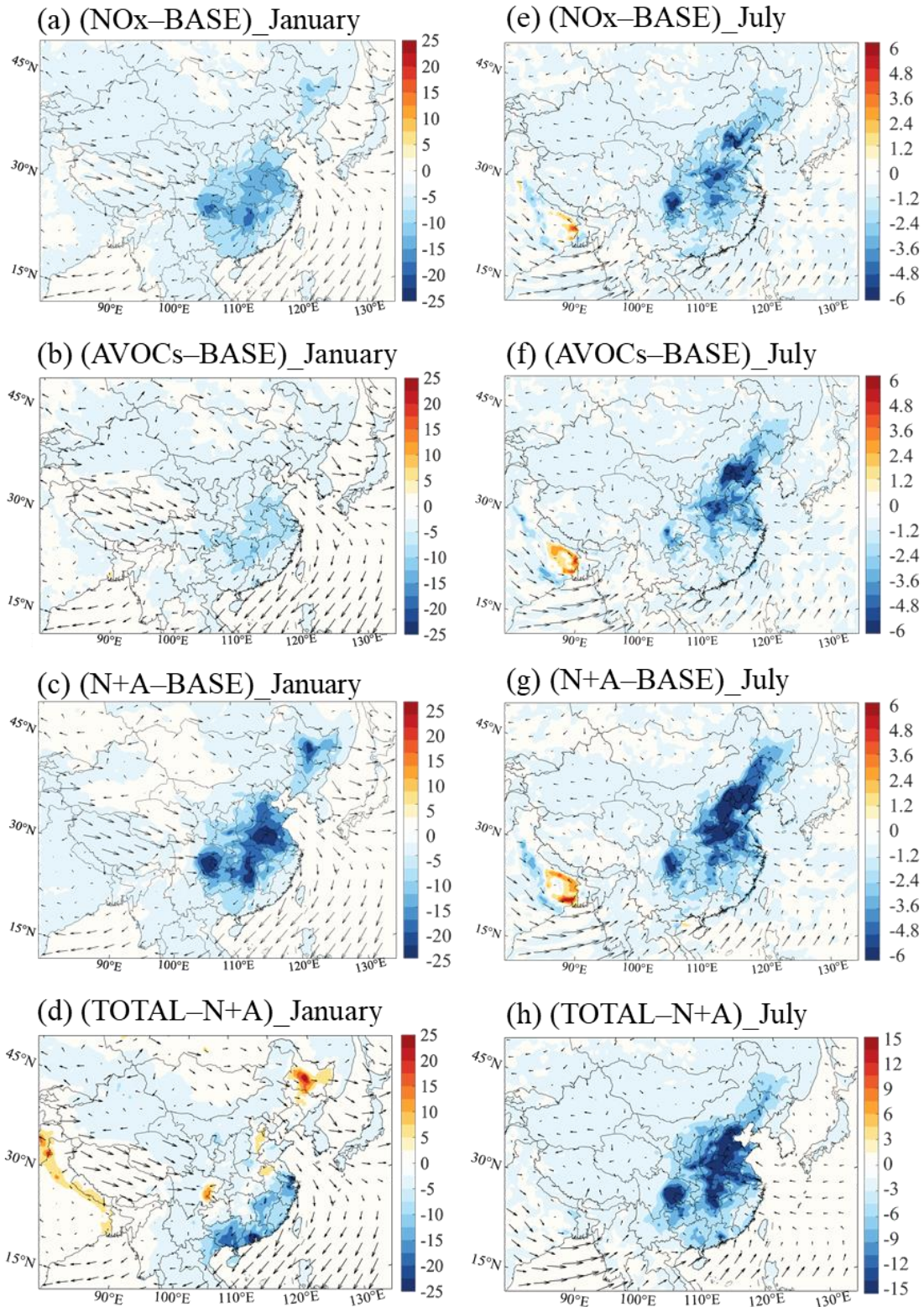
1050

1055

1060

1065

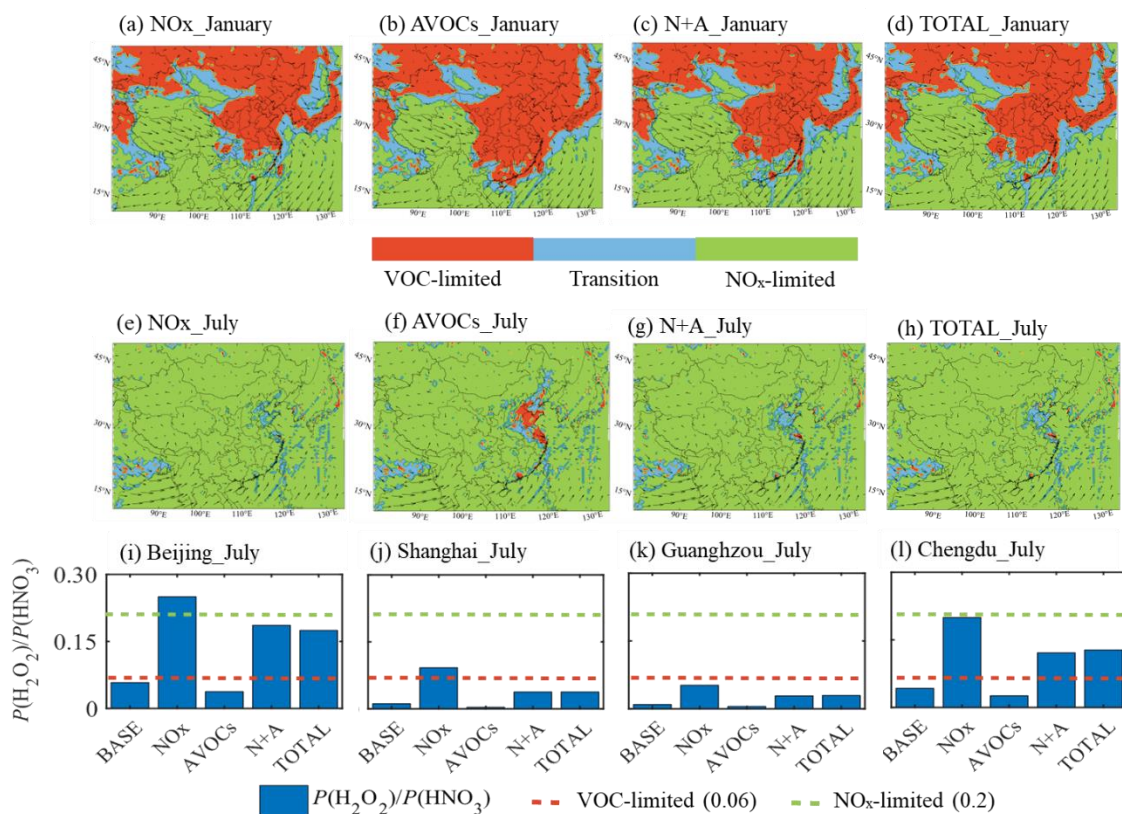




1070 Figure 6. Changes in the monthly-averaged surface concentration of fine particulate aerosol (Unit:  $\mu\text{g m}^{-3}$ ) in response to *NOx* (a, e), *AVOCs* (b, f) and *N+A* case (c, g) relative to *BASE* case and to *TOTAL* case (d, h) relative to *N+A* case for January (a-d) and July (e-h) 2018. Arrows represent the wind speed and wind direction. Notice the inconsistency in the cale of Figure 6h.

1075

1080



1085

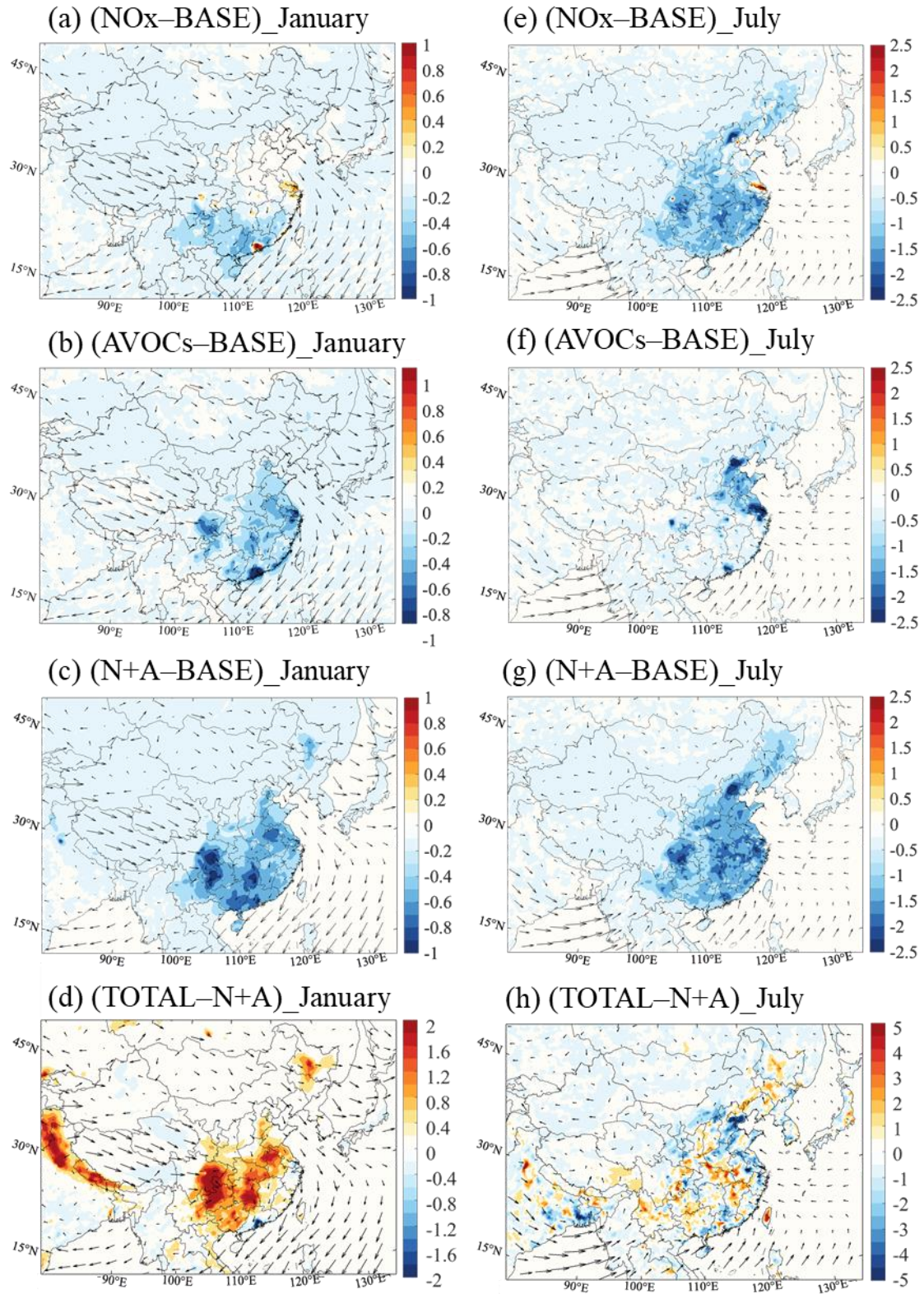
1090

1095

1100

Figure 7. Impact of the emission reduction on ozone sensitivity regimes. (a-h) Display of ozone sensitivity regions in which ozone production is limited by the availability of nitrogen oxides (NO<sub>x</sub>-limited, in green), and volatile organic components (VOC-limited, in red) under the emissions in case of *NO<sub>x</sub>*, *AVOCs*, *N+A*, and *TOTAL* conditions in January (a-d) and July (e-h) of 2018. The regions where ozone production is controlled by the availability of both NO<sub>x</sub> and VOCs (transition) are shown in blue. (i-l) Averaged daytime (06:00 to 19:00 LST) value of the ratio between the production rate of hydrogen peroxide (H<sub>2</sub>O<sub>2</sub>) and nitric acid (HNO<sub>3</sub>) [ $P(\text{H}_2\text{O}_2)/P(\text{HNO}_3)$ ] at four city sites (Beijing, Shanghai, Chengdu, Guangzhou) in the five simulated cases (*BASE*, *NO<sub>x</sub>*, *AVOCs*, *N+A*, and *TOTAL*) for July 2018.





1105 Figure 8. Changes in the monthly-averaged daytime value of atmospheric oxidizing capacity (AOC) response to  $NO_x$  (a, e), AVOCs (b, f), and N+A (c, g) cases relative to BASE case (Unit:  $10^7 \text{ molec. cm}^{-3} \text{ s}^{-1}$ ) and to TOTAL case (d, h) relative to N+A case (Unit:  $10^6 \text{ molec. cm}^{-3} \text{ s}^{-1}$ ) for January (a-d) and July (e-h) 2018.

1110

1115

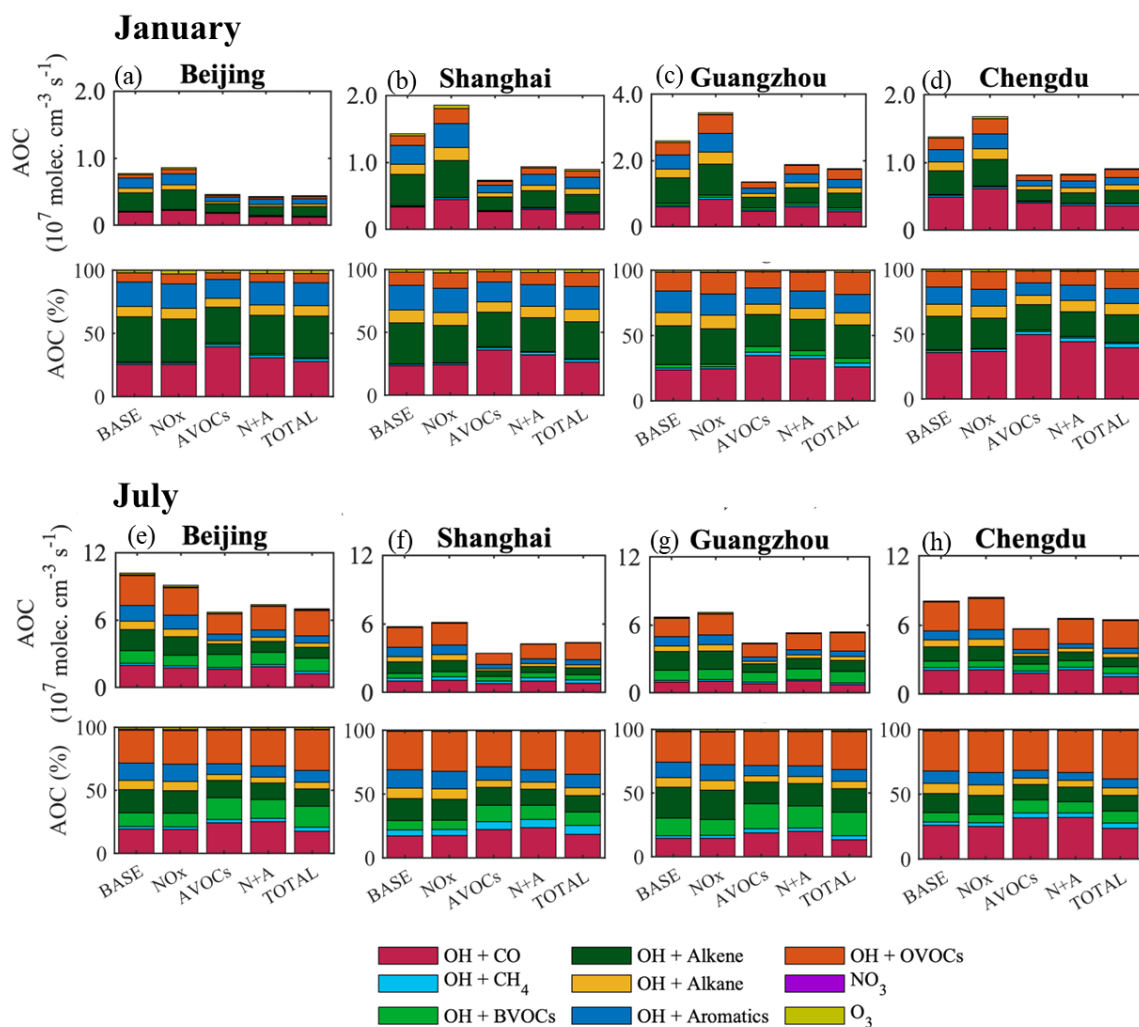
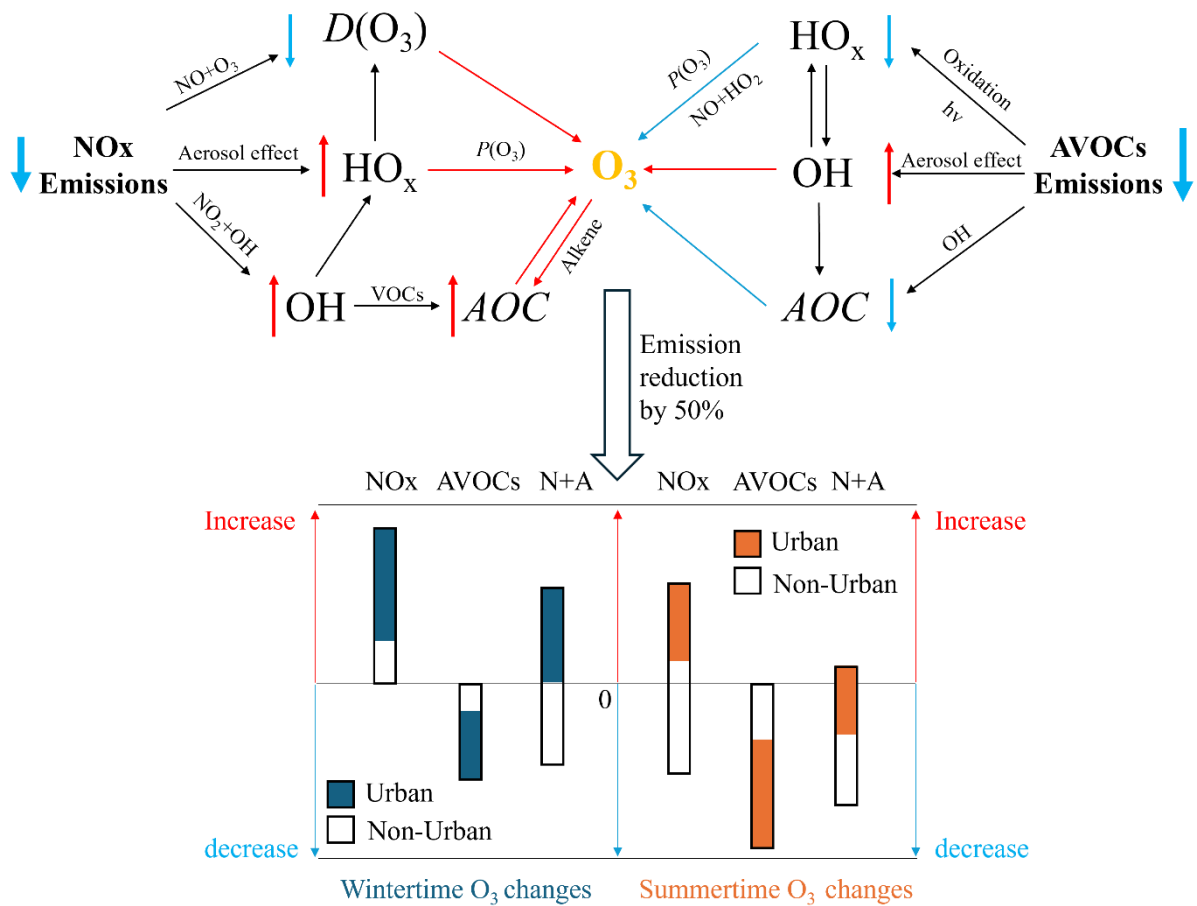


Figure 9. Monthly-averaged value (Unit:  $10^7$  molec.  $\text{cm}^{-3} \text{s}^{-1}$ ) and relative terms (Unit: %) of daytime AOC at the sites of Beijing (a, e), Shanghai (b, f), Guangzhou (c, g), and Chengdu (d, h) in five simulated cases (*BASE*, *NO<sub>x</sub>*, *AVOCs*, *N+A*, *TOTAL* cases) in January (a-d) and July (e-h) of 2018. Notice the inconsistency in the scale of Figure 9c.

1125

1130



1140

Figure 10. Schematics show the responses of oxidative processes, associated with ozone formation, to the reduction in primary emissions of  $NO_x$  and AVOCs in urban areas (VOC-limited) in winter and summer. Arrows besides the chemicals represent the changes associated with the reduction in emission. (decrease trend shown in blue; increase trend shown in red)

1145

Blue and red arrows closing to  $O_3$  represent the positive and negative contributions to the ozone formations.  $AOC$ ,  $P(O_3)$ , and  $D(O_3)$  are the abbreviations of the Atmospheric Oxidative Capacity, production of ozone, and destruction of ozone. Bar figure shows the ranges of ozone changes in whole of China (black bar), in non-urban areas (white part in the bar), and in urban areas (colored part in the bar) in three emissions cases ( $NO_x$ ,  $AVOCs$ , and  $N+A$  represent the case with emission reduction in  $NO_x$ , Anthropogenic VOCs ( $AVOCs$ ), and the combined  $NO_x$  and  $AVOCs$  emissions, respectively) relative to  $BASE$  cases in winter and summer conditions.

1150